The Journal of Neuroscience

https://jneurosci.msubmit.net

JN-RM-1060-23R1

EBF1 limits the numbers of cochlear hair and supporting cells and forms the scala tympani and spiral limbus during inner ear development

Norio Yamamoto, Kyoto Daigaku
Hiroki Kagoshima, Department of Otolaryngology, Head and Neck Surgery, Graduate School of Medicine, Kyoto University, Kyoto, Japan
Hiroe Ohnishi, Department of Otolaryngology, Head and Neck Surgery, Graduate School of Medicine, Kyoto University, Kyoto, Japan
Ryosuke Yamamoto, Biological Sciences, Sunnybrook Research Institute, Sunnybrook Health Sciences Centre, Toronto, ON, Canada
Akiyoshi Yasumoto, Department of Otolaryngology, Head and Neck Surgery, Graduate School of Medicine, Kyoto University, Kyoto, Japan
Yosuke Tona, Department of Otolaryngology, Head and Neck Surgery, Graduate School of Medicine, Kyoto University, Kyoto, Japan
Takayuki Nakagawa, Kyoto Daigaku
Koichi Omori, Kyoto Daigaku

Commercial Interest:

Title:

EBF1 limits the numbers of cochlear hair and supporting cells and forms the scala tympani and spiral limbus during inner ear development

Abbreviated title: EBF1 controls the development of the cochlea

Author names and affiliations:

Hiroki Kagoshima[1], Hiroe Ohnishi[1], Ryosuke Yamamoto[2], Akiyoshi Yasumoto[1], Yosuke Tona[1], Takayuki Nakagawa[1], Koichi Omori[1], and Norio Yamamoto[1,3]

[1]Department of Otolaryngology, Head and Neck Surgery, Graduate School of Medicine, Kyoto University, Kyoto 606-8507, Japan

[2]Biological Sciences, Sunnybrook Research Institute, Sunnybrook Health Sciences Centre, Toronto, ON M4N 3M5, Canada.

[3]Department of Otolaryngology, Kobe City Medical Center General Hospital, Hyogo 650-0047, Japan.

Corresponding Author: Norio Yamamoto, E-mail address: yamamoto@ent.kuhp.kyoto-u.ac.jp

Number of pages: 39

Number of figures: 12

Number of words for abstract: 174 words

Number of words for introduction: 649 words

Number of words for discussion: 1496 words

Conflicts of interest statement: The authors declare that they have no known competing financial interests or personal relationships that could have appeared to influence the work reported in this paper.

Acknowledgements: We thank Dr. Rudolf Grosschedl for providing *Ebf1*$^{-/-}$ and *Ebf1*$^{fl/fl}$ mice, Dr. Ryoichiro Kageyama for providing *Atoh1* ISH probe, and Center for Anatomical, Pathological and Forensic Medical Research, Graduate School of Medicine, Kyoto University for preparing hematoxylin-eosin staining slides. This study was supported by JSPS KAKENHI (grant number: JP22H03234) awarded to NY.

Abstract

Early B-cell factor 1 (EBF1) is a basic helix-loop-helix transcription factor essential for the differentiation of various tissues. Our single-cell RNA sequencing data suggest that *Ebf1* is expressed in the sensory epithelium of the mouse inner ear. Here, we found that the murine *Ebf1* gene and its protein are expressed in the prosensory domain of the inner ear, medial region of the cochlear duct floor, otic mesenchyme, and cochleo-vestibular ganglion. *Ebf1* deletion in mice results in incomplete formation of the spiral limbus and scala tympani, increased number of cells in the organ of Corti and Kölliker's organ, and aberrant course of the spiral ganglion axons. *Ebf1* deletion in the mouse cochlear epithelia caused the proliferation of SOX2-positive cochlear cells at E13.5, indicating that EBF1 suppresses the proliferation of the prosensory domain and cells of Kölliker's organ to facilitate the development of appropriate numbers of hair and supporting cells. Furthermore, mice with deletion of cochlear epithelium-specific *Ebf1* showed poor postnatal hearing function. Our results suggest that *Ebf1* is essential for normal auditory function in mammals.

Significance statement

The elaborate cellular organization and three-layered luminal structure of the mammalian cochlea are essential for normal sound perception, but the developmental process of these structures is not fully understood. The present study revealed the roles of the basic helix-loop-helix type transcription factor *Ebf1* in the development of the cochlea. *Ebf1* was widely expressed in the inner ear, regulated the proper number of cochlear hair and supporting cells, and was involved in developing scala tympani and spiral limbus. As a result, *Ebf1* was necessary for the development of normal hearing. These results suggest the essential roles of *Ebf1* in the whole

cochlear development and contribute to understanding a part of the complex cochlear development process.

Introduction

The inner ear is a unique and complex organ that consists of bony and membranous labyrinths. The membranous labyrinth contains multiple sensory organs, including the cochlea and several vestibular organs. The cochlea is responsible for hearing and comprises three compartments (scalae): the scala vestibuli, scala tympani, and scala media. The scala vestibuli and scala tympani develop from the mesenchyme surrounding the inner ear (Sher, 1971). The scala media is situated between the scala vestibuli and scala tympani and contains sensory epithelia that transduce sound into electrical signals via specialized sensory cells known as hair cells. Cochlear hair cells are located within the organ of Corti in the middle part of the scala media epithelium, and consist of one row of inner hair cells and three rows of outer hair cells. These hair cells are surrounded by several types of non-sensory supporting cells, including pillar and Deiters' cells. The precise number and placement of mechanosensory hair cells and non-sensory supporting cells enable the accurate reception of mechanical stimulation of sound and its conversion into neural signals.

Inner ear development in mice begins with the formation of an ectodermal thickening called the otic placode, which is located adjacent to the hindbrain (Wu and Kelley, 2012). The otic placode invaginates to form a spherical structure called an otocyst at approximately embryonic day (E) 9.5. The ventral side of the otocyst forms the future sensory epithelium, where the sex-determining region Y-box transcription factor 2 (*Sox2*) is expressed (Kiernan et al., 2005). At E10.5, the cochlear and endolymphatic ducts and semicircular canals begin to form on the

ventral and dorsal sides of the otocyst, respectively. The ventral side of the cochlear duct (cochlear duct floor) begins to develop into a future sensory domain by expressing *Sox2* and *Jagged1* at E11.5 (Wu and Kelley, 2012). The *Sox2*-positive region becomes limited to the middle part of the ventral cochlear duct and is recognized as a prosensory domain at E13.5 and E14.5 (Kiernan et al., 2005; Ohyama et al., 2010). The region medial to the prosensory domain toward the axis of the cochlea (modiolus) is called the greater epithelial ridge (GER) and transiently contains Kölliker's organ, which is composed of columnar supporting cells during the developmental stage and becomes the inner sulcus with cuboidal cells and the spiral limbus with interdental cells in the mature cochlea (Dayaratne et al., 2014). Additionally, the GER is a source of sensory epithelia and has the potential to produce sensory cells after the establishment of hair cells (Kubota et al., 2021).

The complex cellular structure and developmental processes of the inner ear depend on the highly regulated expression patterns of signaling molecules and transcription factors. However, the mechanisms underlying inner ear development are not fully understood. To comprehensively elucidate these mechanisms, we analyzed the single-cell RNA-seq data of the inner ear epithelial cells. In this study, we found that the early B-cell factor 1 gene (*Ebf1*) was upregulated in clusters of sensory epithelial progenitors, and confirmed that it was expressed on the medial side of the cochlear duct floor, the prosensory area of the vestibular macula and crista, and the spiral ganglion (Yamamoto et al., 2021).

EBF1 belongs to the EBF family of transcription factors, which are basic helix-loop-helix (bHLH) transcription factors (Hagman et al., 1995), and encodes four paralogous genes in mammals (Liberg et al., 2002). Similar to other bHLH transcription factors, EBF1 is involved in

various developmental processes, including the determination of cell fate and differentiation of B lymphocytes and olfactory epithelia (Liberg et al., 2002).

Considering the various roles of EBF1 as a bHLH transcription factor and the importance of bHLH transcription factors－such as ATOH1—in inner ear development, we analyzed the function of EBF1 in inner ear development. In the present study, we confirmed the spatiotemporal expression of *Ebf1* during inner ear development and examined the effects of *Ebf1* deletion on inner ear development and hearing.

Material and Methods

Animals

Slc: ICR mice were purchased from Japan SLC (Hamamatsu, Japan). $Ebf1^{-/-}$ mice (Lin and Grosschedl, 1995) and $Ebf1^{fl/fl}$ (Gyory et al., 2012) were used in this study. $Ebf1^{fl/+}$ mice were crossed with $Foxg1^{Cre/+}$ *mice* (*Foxg1Cre*) (Hébert and McConnell, 2000) and $Ebf1^{-/-}$ or *Foxg1Cre;*$Ebf1^{fl/fl}$ mice were used as experimental animals. Additionally, we used $Ebf1^{+/+}$ and $Ebf1^{+/-}$ mice as controls of $Ebf1^{-/-}$ mice and *Foxg1Cre;*$Ebf1^{fl/+}$ mice as controls of *Foxg1Cre;*$Ebf1^{fl/fl}$ mice.

$Ebf1^{+/-}$, *Foxg1Cre*, and $Ebf1^{fl/fl}$ mice were maintained on a C57BL/6 background. All experimental protocols were approved by the Animal Research Committee of Kyoto University (Med Kyo 20132, Kyoto, Japan). All animal experiments were performed according to the National Institutes of Health Guidelines for the Care and Use of Laboratory Animals. All the animals used in this study were maintained at the Institute of Laboratory Animals, Graduate School of Medicine, Kyoto University. The mice were mated in the evening, and vaginal plugs were checked early in the morning. The day a vaginal plug was detected was defined as E0.5.

Quantitative reverse transcription polymerase chain reaction (qRT-PCR)

Inner ears were dissected from E9.5, E10.5, E11.5, E12.5, E13.5, E14.5, E16.5, E18.5, and postnatal day (P) 0 ICR mice. After the surrounding tissue was removed from the inner ears, at least four samples were immersed in TRIzol™ Reagent (15596018, Thermo Fischer Scientific, Waltham, MA, USA) and preserved at −80 ℃ until RNA extraction. Total RNA was extracted using the RNeasy™ Mini Kit (74104, QIAGEN, Venlo, Netherlands) and reverse transcribed using the ReverTra Ace™ qPCR RT Master Mix with gDNA Remover (FSQ-301, TOYOBO, Osaka, Japan). The cDNA was mixed with PowerUp SYBR Green Master Mix (A25742, Applied Biosystems, Waltham, MA, USA) and various sets of gene-specific forward and reverse primers and subsequently subjected to real-time PCR quantification using a StepOnePlus™ Real-Time PCR System (4376373, Applied Biosystems). The following primer sequences were used: *Ebf1* forward, AACTCCAAGCACGGGCGGAG; *Ebf1* reverse, CGGGCTGATGGCTTTGATACAGG; *Rplp0* forward, CACTGGTCTAGGACCCGAGAAG; *Rplp0* reverse, GGTGCCTCTGGAGATTTTCG. Relative mRNA expression levels were calculated using the standard curve method, and the mouse housekeeping gene *Rplp0* was used as an invariant control.

***in situ* hybridization (ISH)**

Whole embryos (E9.5–E11.5) and whole heads (E12.5–P0) were fixed in 4% paraformaldehyde (PFA; 02890-45, Nacalai Tesque, Kyoto, Japan) in 0.1 M phosphate-buffered saline (PBS; 162-19321, FUJIFILM Wako Pure Chemical Corporation, Osaka, Japan) at 4 ℃ overnight. Samples were cryoprotected in 30% sucrose (30403-55, Nacalai Tesque)/PBS, embedded in Tissue-Tek®

O.C.T.™ compound (4583, Sakura Finetek Japan, Tokyo, Japan), and sectioned at 10-μm thickness using a cryostat (CryoStar™ NX70; MIC956960, Thermo Fisher Scientific). The sections were subsequently mounted on silane-coated glass slides (SMAS-01, Matsunami Glass, Osaka, Japan).

cDNA fragments were generated by PCR using E13.5 inner ear cDNA of Slc:ICR mice and subsequently cloned into the pCR®-Blunt II-TOPO® vector (451245, Invitrogen, Waltham, MA, USA) to prepare RNA probe templates. We synthesized digoxigenin (DIG)-labeled sense and antisense RNA probes using a DIG RNA Labeling Kit (11175033910, Roche, Basel, Switzerland) after digestion with the appropriate restriction enzymes *Bam*HI-HF, *Hind*III, *Not*I-HF, *Sac*I, or *Xho*I (R3136S, R0104S, R3189S, R0156S, R0146S, New England Biolabs, Ipswich, MA, USA). The following probes were used for ISH: *Ebf1* (NM_001,290,709, nucleotides 1436–2269), *Sox2* (IMAGE clone: 6413283), *Bmp4* (NM_007554.3, nucleotides 1013-1876), *Atoh1* (NM_007500.5, nucleotides 13-2111), and *Fgf10* (NM_008002.5, nucleotides 571-1027). Each corresponding sense probe was used as a negative control.

Sections were fixed with 4% PFA and 0.2% glutaraldehyde (17025-25, Nacalai Tesque) in PBS at room temperature (RT) for 10 min, bleached with 6% hydrogen peroxidase (081-04215, FUJIFILM Wako Pure Chemical Corporation) in 0.1% Tween-20 (sc-29113, Santa Cruz Biotechnology, Dallas, TX, USA) in PBS (PBST) at RT for 10 min, treated with 20 μg/μL proteinase K (3115879001, Roche) for 5 min, and re-fixed with 4% PFA and 0.2% glutaraldehyde in PBS at RT for 10 min.

The prehybridization was performed in hybridization solution containing 50% formamide (13015-75, Nacalai Tesque), 5× saline sodium citrate buffer (SSC, 32146-91, Nacalai Tesque; adjusted to pH 4.5 with citrate), 1% sodium dodecyl sulfate (71736-500ML , Sigma-Aldrich, St.

Louis, MO, USA), 50 μg/mL yeast RNA (AM7118, Invitrogen), and 50 μg/mL heparin (H9399-100KU, Sigma-Aldrich) at 70 ℃ for 1 h. For hybridization, we incubated the sections in a hybridization solution with a 0.2 μg/mL DIG-labelled RNA probe at 70 ℃ for 16 h in sealed plastic bags.

Sections were rinsed first in 50% formamide with 6× SSC and 1% sodium dodecyl sulfate at 70 ℃, then in 50% formamide with 2.4× SSC at 65 ℃, and finally in 1× Tris-buffered saline (35438-81, Nacalai Tesque) with 0.1% Tween 20 (TBST) at RT. Sections were blocked with 5% sheep serum (S2263-500ML, Sigma-Aldrich) and incubated with a 1:4000 dilution of Anti-Digoxigenin-AP Fab fragments (11093274910, Roche) at 4 ℃ overnight.

After rinsing with TBST and NTMT containing 100 mM NaCl (31334-51, Nacalai Tesque), 100 mM Tris-HCl pH 9.5, 10 mM $MgCl_2$ (133-00161, FUJIFILM Wako Pure Chemical Corporation), 0.1% Tween-20, and 480 μg/mL levamisole (16595-80-5, Sigma-Aldrich), the sections were incubated with nitro-blue tetrazolium chloride (11383213001, Roche) and 5-bromo-4-chloro-3-indolyl phosphate solution (B6777-100MG, Roche). Images were captured using a BX-50 microscope (Olympus Corp., Tokyo, Japan).

Immunohistochemistry (IHC) analysis

IHC sections were prepared in a manner similar to that used for ISH. After washing with PBS, all samples were incubated with Blocking One Histo (06349-64, Nacalai Tesque) for 10 min at RT and 10% normal donkey serum (D9663-10ML, Sigma-Aldrich) in PBS/0.5% Triton X- 100 with 5% Blocking One Histo for 30 min at RT. The samples were stained with primary antibodies at 4 ℃ overnight or RT for 1 h. After washing with PBST, the samples were incubated with Alexa Fluor secondary antibodies. F-actin (actin filaments) was stained with phalloidin 647

(1:500; A22287, Thermo Fisher Scientific) at RT for 1 h. Nuclei were stained with 4′,6-diamidino-2-phenylindole (DAPI; D1306, Thermo Fisher Scientific).

The following primary antibodies were used in this study: rabbit anti-EBF1 antibody (1:1000, AB10523, RRID: AB_2636856; Millipore, Darmstadt, Germany,), mouse anti-MYO7A antibody (1:1000, 138-1; Developmental Studies Hybridoma Bank, Iowa City, IA, USA), rabbit anti-MYO7A antibody (1:1000, 25-6790, RRID: AB_10015251; Proteus BioSciences, Waltham, MA, USA), goat anti-SOX2 antibody (1:250, AF201, RRID: AB_355110; R&D Systems, Minneapolis, MN, USA), rabbit anti-SOX2 antibody (1:100, 11064-1-AP, RRID: AB_2195801; Proteintech, Manchester, UK), rabbit anti-VGLUT3 antibody (1:500, 135 203, RRID:AB_887886; Synaptic systems, Goettingen, Germany), goat anti-JAG1 antibody (1:500, sc-6011, RRID: AB_649689; Santa Cruz Biotechnology), mouse anti-p27Kip1 antibody (1:200, 610242, RRID: AB_397637; BD Biosciences, Franklin Lakes, NJ, USA), rabbit anti-Tubulin β 3 (TUJ1) antibody (1:1000, PRB-435P, RRID: AB_291637; Biolegend, San Diego, CA, USA), rabbit anti-PROX1 antibody (1:500, AB5475, RRID: AB_177485; Millipore), rabbit Anti-Nerve Growth Factor Receptor Antibody, p75 antibody (1:500, AB1554, RRID: AB_11211656; Millipore), rabbit anti-BLBP (FABP7) antibody (1:200, ab32423, RRID:AB_880078: Abcam, Cambridge, UK) and rabbit anti-cleaved caspase 3 (Asp175) antibody (1:400, 9661, RRID: AB_2341188; Cell Signaling Technology, Danvers, MA, USA).

Antigen retrieval was performed for CDKN1B (mouse anti-p27Kip1 antibody) staining by heating sections in HistoVT one (06380-76, Nacalai Tesque) at 90 ℃ for 10 min prior to the addition of the primary antibodies.

The secondary antibodies used were Alexa Flour 488 donkey anti-rabbit IgG, Alexa Flour 488 donkey anti-goat IgG, Alexa Flour 488 donkey anti-mouse IgG, Alexa Flour 568 donkey anti-

rabbit IgG, Alexa Flour 568 donkey anti-goat IgG, Alexa Flour 647 donkey anti-rabbit IgG, Alexa Flour 647 donkey anti-goat IgG, and Alexa Flour 647 donkey anti-mouse IgG (1:500; A21206, A11055, A21202, A10042, A11057, A31573, A21447, A31571, Thermo Fisher Scientific).

The sections were mounted using Fluoromount-G® Anti-Fade (0100-35, Southern Biotechnology Associates Inc., Birmingham, AL, USA). Images of the specimens were captured using an Olympus BX50 microscope (Olympus), an Olympus DP70 digital camera (Olympus), and a Zeiss LSM900 with Airyscan2 (Carl Zeiss AG, Oberkochen, Germany).

Hematoxylin-eosin (HE) staining

Freshly isolated E18.5 mouse head were immediately fixed by 10% formaldehyde and embedded in paraffin. Paraffin sections (3-μm thick) were immersed in Hematoxylin monohydrate (1.15938, Sigma-Aldrich) at RT for 7.5 min and in Eosin Y (115935, Sigma-Aldrich) at RT for 2 min. Dehydration was performed using graded ethanol solutions (70%, 90%, and three times of 100%) and clearing was performed three times using xylene.

Cochlea whole-mount preparation

The inner ears were dissected from mice heads at E18.5 and fixed in 4% PFA in PBS at RT for 1 h. After fixation and before primary antibody staining, the outer membrane, including the Reissner's membrane, was removed to expose the organs of Corti. After staining with a secondary antibody, the organ of Corti was dissected and mounted on a glass slide for imaging.

Proliferation and apoptosis assays

241 Cell proliferation in the cochlea was assessed by detecting the incorporated 5-ethynyl-2'-
242 deoxyuridine (EdU) (A10044, Thermo Fisher Scientific) on frozen sections. EdU was detected
243 using the Click-iT™ Plus EdU Cell Proliferation Kit for Imaging Alexa 555 Dye (C10638,
244 Thermo Fisher Scientific), according to the manufacturer's instructions. Pregnant mice were
245 injected with EdU at E12.5, E13.5, and E14.5 (three injections at 50 μg/g at 2-h intervals) and at
246 E16.5 (a single injection at 100 μg/g). E12.5, E13.5, and E14.5 embryos were collected 8 h after
247 the first injection. E16.5 embryos were collected 4 h after the injection. The basal or basal-to-
248 middle regions of the cochlear duct were observed at E12.5 or at E13.5, E14.5, and E16.5,
249 respectively.
250 Apoptotic cells were detected by identifying the expression of cleaved caspase 3 (CC3) in frozen
251 sections via IHC staining.
252
253 **Auditory brainstem response (ABR) and distortion product of otoacoustic emissions**
254 **(DPOAE)**
255 ABR measurements were performed under general anesthesia as described previously (Kada et
256 al., 2009) at P21 (n = 3 for each genotype). The thresholds for 10, 20, and 40 kHz were
257 determined based on the responses at different intensities with 5 dB sound pressure level
258 intervals. DPOAE recordings were performed as described previously (Hamaguchi et al., 2012)
259 at P21 (n = 4 for each genotype). Two primary tones (f1, f2, f1<f2) were used as input signals,
260 with f2 set at eight frequency points (4, 6, 8, 12, 16, 24, 32, and 40 kHz), maintaining a
261 frequency ratio of f2/f1 = 1.2. The intensity levels of the stimulatory sounds were 65 and 55 dB
262 sound pressure level for f1 and f2, respectively. DPOAE was detected as a peak at 2f1–f2 in the
263 spectrum.

Quantification

Cell quantification and measurements were performed at E18.5 using the Cell Counter plugin of ImageJ (Schneider et al., 2012). The total length of the cochlea was measured based on the region with MYO7A-positive hair cells from the basal to apical turns. Cochlear hair cells were identified by phalloidin and MYO7A labeling. Two types of cells, PROX1- and SOX2-positive cells, were counted to quantify the supporting cells of the cochlea. The cochlear duct was divided into three regions: basal, middle, and apical, and we selected the 200 μm length in each region for MYO7A- and PROX1-positive cells and 100 μm in the basal region for SOX2-positive cells from the center part of each region and counted the number of cells within the selected part. To determine the number of cochlear hair cells and supporting cells in the entire length of the cochlea, the number of MYO7A-positive and PROX1-positive cells was counted, respectively.

Experimental design and statistical analysis

For all statistical analyses, at least three samples from each experimental group were analyzed. Student's *t*-test was used to determine the differences between two experimental groups. One-way or two-way analysis of variance was performed to assess the differences between more than two experimental groups and *p*-values less than 0.05 were considered statistically significant. Statistical analyses were performed using R version 4.2.2 (2022-10-31). All details of statistical analyses are provided in the figures and legends.

Results

Ebf1 is expressed in developing mouse inner ears

In silico analysis of embryonic inner ear epithelia suggested that *Ebf1* is predominantly expressed in the inner ear sensory epithelium during early development (Yamamoto et al., 2021). To quantify *Ebf1* expression at each stage of inner ear development, we performed qRT-PCR using whole embryonic inner ears from E9.5 to P0 (Fig. 1A, $F(8, 18) = 5.39$, $p = 0.001$, one-way ANOVA with Tukey–Kramer *post-hoc* test). The expression of *Ebf1* mRNA transcripts began to increase at E10.5 and reached a maximum at E13.5 (Fig. 1A, $p = 0.00108$). The relative expression level at E13.5 was approximately 10-fold higher than that at E9.5. The expression level then decreased but remained 7.5 times higher than that at E9.5 even at P0 (Fig. 1A, $p = 0.0154$).

To describe the spatiotemporal expression patterns of *Ebf1* during inner ear development, we performed ISH (Fig. 1 B, C) and IHC (Fig. 2A) analyses on sections of the developing inner ear of wild-type mice at various embryonic stages. We stained *Sox2*, which is expressed in the sensory progenitor region of the inner ear from the early developmental stages (Kiernan et al., 2005), as well as *Ebf1* on adjacent sections to specify the location of *Ebf1* expression, and compared the expression of the two genes and their products.

First, we examined *Ebf1* expression at E13.5 (Fig. 1B), which is when the sensory epithelium of the inner ear forms and *Ebf1* expression level is maximized during inner ear development (Fig. 1A). *Ebf1* was expressed on the medial side of the cochlear duct floor, including the prosensory domain (white arrows in Fig. 1B), spiral ganglion (white asterisks in Fig. 1B), otic mesenchyme (black asterisks in Fig. 1B), and parts of the prosensory regions of the vestibule and crista (black arrows in Fig. 1B). Compared with *Sox2*, *Ebf1* was expressed more medially within the cochlear duct floor, which developed into Kölliker's organ and the organ of Corti, and its expression in the vestibule was more restricted (Fig. 1B).

Subsequently, we examined the spatiotemporal expression of *Ebf1* throughout inner ear development, including the onset of expression in the inner ear epithelium, using inner ear sections from E9.5 to P0 (Fig. 1C). At E9.5, *Ebf1* was not expressed in the otocyst but was expressed in the progenitor cells of the cochleo-vestibular ganglion (CVG) (white asterisk in Fig. 1C, E9.5), which delaminate from the ventral side of the otocyst into the otic mesenchyme (Wu and Kelley, 2012). At E10.5, *Ebf1* expression was observed on the ventromedial side of the otocyst, which develops into the cochlear duct, and in the ventrolateral epithelium of the otocyst, which develops into the crista (black arrowheads in Fig. 1C, E10.5). Additionally, *Ebf1* expression was detected in the otic mesenchyme (black asterisk in Fig. 1C, E10.5) and CVG (white asterisk in Fig. 1C, E10.5), which persisted until later stages (Fig. 1C). *Ebf1* was expressed in the border region, where the cochlear duct begins to elongate, at E11.5 (white arrow in Fig. 1C, E11.5), in the medial side of the cochlear duct floor at E12.5 (white arrow in Fig. 1C, E12.5), and in the future crista region in the vestibule at E11.5 and 12.5 (black arrows in Fig. 1C, E11.5 and E12.5). In the cochlea at E16.5 and E18.5, *Ebf1* was expressed throughout the organ of Corti and Kölliker's organ (Fig. 1C, E16.5 and E18.5), whereas *Sox2* was expressed in the organ of Corti and the lateral half of Kölliker's organ (Fig. 1C E16.5 and E18.5), consistent with a previous report (Urness et al., 2015). *Ebf1* was expressed in the spiral ligaments, tympanic border cells (white arrowheads in Fig. 1C, E18.5) (Taniguchi et al., 2012), vestibules, and crista (Fig. 1C, E18.5). *Ebf1* expression was maintained until P0 (Fig. 1C, P0).

IHC analysis showed that EBF1 was expressed throughout Kölliker's organ and the prosensory domain, whereas SOX2 was expressed in a part of Kölliker's organ and the prosensory domain (upper panels of Fig. 2A), which is consistent with the ISH results. The disappearance of the EBF1 signal from the cochlear epithelia and mesenchyme in conventional *Ebf1* knockout (*Ebf1*$^{-/-}$

) mice confirmed the specificity of the anti-EBF1 antibody used in this study (lower panels of Fig. 2A).

Ebf1 deletion altered the structure of the cochlear duct

Our ISH and IHC analyses, which showed the expression of *Ebf1* and its protein in both the developing inner ear epithelia and mesenchyme, suggest that *Ebf1* is involved in the development of both the inner ear sensory epithelium and otic mesenchyme. We used two mutant mouse strains to examine the roles of *Ebf1* in developing inner ears: an *Ebf1* conventional knockout (*Ebf1*$^{-/-}$) mouse (Lin and Grosschedl, 1995) and a Foxg1-Cre-mediated inner ear epithelia-specific conditional knockout mouse (*Foxg1Cre;Ebf1*$^{fl/fl}$) (Hébert and McConnell, 2000; Gyory et al., 2012) in which *Ebf1* expression persists in the inner ear mesenchyme (arrows in Fig. 2B).

Comparison of the gross morphology of the membranous labyrinth of the inner ear at E18.5 revealed no difference between *Ebf1*$^{+/+}$ and *Ebf1*$^{-/-}$ mice (Fig. 3A). However, after removing the lateral wall and Reissner's membrane of the cochlea to expose the cochlear duct floor, we found that *Ebf1*$^{-/-}$ mice had a shorter cochlear duct than *Ebf1*$^{+/+}$ mice (white arrowhead in Fig. 3B).

HE staining of the cochlea at E18.5 revealed incomplete formation of the scala tympani, particularly in the middle and apical regions of the cochlea of *Ebf1*$^{-/-}$ mice compared with those of control mice (arrowheads in Fig. 3C). Moreover, a spiral limbus is hypoplastic in the basal region and aplastic in the other regions of the cochlea in *Ebf1*$^{-/-}$ mice (sl; Fig. 3C); a lower number of cochlear turns was also observed in the cochlear sections of these mice (arrows in the upper right panels in Fig. 3C), supporting the gross morphological observations.

Ebf1 was expressed in the otic mesenchyme from early to later developmental stages. To elucidate whether the hypoplastic scala tympani, fewer cochlear turns, and lack of spiral limbus were caused by the *Ebf1*-deficient mesenchyme, we examined the cochlear morphology of *Foxg1Cre;Ebf1*$^{fl/fl}$ and *Foxg1Cre;Ebf1*$^{fl/+}$ mice via HE staining. In contrast to the hypoplastic scala tympani of *Ebf1*$^{-/-}$ mice, the scala tympani of *Foxg1Cre;Ebf1*$^{fl/fl}$ mice was formed in the whole cochlear turns (right panels of Fig. 3C). The number of cochlear turns in *Foxg1Cre;Ebf1*$^{fl/fl}$ mice was similar to that in the control mice (*Foxg1Cre;Ebf1*$^{fl/+}$ mice). However, *Foxg1Cre;Ebf1*$^{fl/fl}$ mice lacked a spiral limbus, as observed in *Ebf1*$^{-/-}$ mice (Fig. 3C). To quantify the area of a spiral limbus, we performed the IHC of FABP7 (Fig. 3D), which is expressed in a spiral limbus (Saino-Saito et al., 2010). The area of a spiral limbus was significantly smaller in basal and middle turns of *Ebf1*$^{-/-}$ and *Foxg1Cre;Ebf1*$^{fl/fl}$ mice compared with their control mice (Fig. 3E, *Ebf1*$^{+/+}$ vs *Ebf1*$^{-/-}$: basal region ($t(6) = 8.92$, $p = 1.10e\text{-}4$), middle region ($t(6) = 16.8$, $p = 2.85e\text{-}6$); *Foxg1Cre;Ebf1*$^{fl/+}$ vs *Foxg1Cre;Ebf1*$^{fl/fl}$: basal region ($t(6) = 11.0$, $p = 3.43e\text{-}5$), middle region ($t(6) = 12.8$, $p = 1.38e\text{-}5$), Student's *t*-test). These results suggest that epithelial *Ebf1* does not control the formation of scala tympani and cochlear turns but mesenchymal *Ebf1* supposedly does. In contrast, EBF1 within the epithelia is somehow involved in the spiral limbus formation.

Ebf1 deletion caused an increase in the number of cochlear hair, supporting, and Kölliker's organ cells

Observation of the cochlear epithelia in HE-stained samples revealed that both *Ebf1*$^{-/-}$ and *Foxg1Cre;Ebf1*$^{fl/fl}$ mice had deformed Kölliker's organs and organs of Corti (Ko and oC in Fig.

3C). To examine these phenotypes more comprehensively, we performed IHC analysis on inner ear sections and cochlear whole-mount samples from E18.5 (Fig. 4).

IHC analysis of cochlear sections showed that *Ebf1* deletion increased the number of MYO7A-positive hair cells as well as SOX2-positive supporting and Kölliker's organ cells from the basal to the apical region at E18.5 in both *Ebf1*$^{-/-}$ and *Foxg1Cre;Ebf1*$^{fl/fl}$ mice (Fig. 4A). An increase in the number of SOX2-positive cells within the medial region of the cochlear duct floor was also observed at E14.5 (arrowhead in Fig. 2A). In contrast, *Ebf1* deletion had no morphological effects on the vestibular sensory epithelium (data not shown). Additionally, the apical region of *Ebf1*$^{-/-}$ mouse cochleae contained multiple layers of SOX2-positive cells (asterisk in Fig. 4A). IHC analysis of whole-mount cochlear samples showed that *Ebf1*$^{-/-}$ and *Foxg1Cre; Ebf1*$^{fl/fl}$ mice had an increased number of MYO7A-positive hair cells (Fig. 4B) and ectopic MYO7A-positive cells within the GER (arrows in Fig. 4B). Although the normal cochlea has one and three rows of inner and outer hair cells, respectively, the mutant cochlea had eight to nine rows of hair cells. We found ectopic hair cells in 7 of the 12 examined *Ebf1*$^{fl/fl}$ mice cochleae. These ectopic MYO7A-positive cells contained stereocilia-like structures, as indicated by phalloidin staining (arrows in Fig. 4C). Increased numbers of supporting cells were confirmed in whole-mount cochlear samples by IHC staining of SOX2 (Fig. 4B), a supporting and Kölliker's organ cell marker, and PROX1 (Fig. 4D), a pillar and Deiters' cell marker (Bermingham-McDonogh et al., 2006).

To quantify the number of hair and supporting cells, we counted the cells in three regions within the cochlea (basal, middle, and apical regions; Fig. 5A) and measured the number of MYO7A- or PROX1-positive cells per 200 μm or all cells within the whole cochlea in *Ebf1*$^{fl/fl}$ mice and control mice at E18.5. For SOX2-positive cells, we counted the cell number per 100 μm only in

the basal regions at E18.5. The results showed that the cochlear hair cell number was significantly increased in *Ebf1*$^{-/-}$ mice compared to *Ebf1*$^{+/+}$ mice in all three regions (Fig. 5B) and the whole cochleae (Fig. 5C). *Ebf1*$^{+/-}$ mice exhibited a significantly higher number of cochlear hair cells than *Ebf1*$^{+/+}$ mice in the middle and apical regions (Fig. 5B, $F(4,27) = 9.43$, $p = 6.64e\text{-}5$, two-way ANOVA with Bonferroni *post-hoc* test). The hair cell numbers per 200 μm of *Ebf1*$^{+/+}$, *Ebf1*$^{+/-}$, and *Ebf1*$^{-/-}$ mice were 142.3 ± 9.0, 150.0 ± 2.8, and 367.5 ± 30.8 in the basal regions (*Ebf1*$^{+/+}$ vs *Ebf1*$^{+/-}$: $p = 1.0$; *Ebf1*$^{+/+}$ vs *Ebf1*$^{-/-}$: $p = 3.17e\text{-}17$; *Ebf1*$^{+/-}$ vs *Ebf1*$^{-/-}$: $p = 7.69e\text{-}17$); 152.8 ± 8.1, 190.3 ± 7.0, and 363.0 ± 22.4 in the middle regions (*Ebf1*$^{+/+}$ vs *Ebf1*$^{+/-}$: $p = 7.67e\text{-}3$: *Ebf1*$^{+/+}$ vs *Ebf1*$^{-/-}$: $p = 1.81e\text{-}16$; *Ebf1*$^{+/-}$ vs *Ebf1*$^{-/-}$: $p = 2.33e\text{-}14$) and 154.5 ± 5.1, 183.5 ± 6.8, and 440.3 ± 23.8 in the apical regions (*Ebf1*$^{+/+}$ vs *Ebf1*$^{+/-}$: $p = 4.79e\text{-}2$; *Ebf1*$^{+/+}$ vs *Ebf1*$^{-/-}$: $p = 7.07e\text{-}20$; *Ebf1*$^{+/-}$ vs *Ebf1*$^{-/-}$: $p = 1.12e\text{-}18$), respectively. The number of *Ebf1*$^{+/+}$ and *Ebf1*$^{-/-}$ hair cells in the whole cochlea were 2559.3 ± 108.0 and 4302.0 ± 194.2, respectively (Fig. 5C, $t(4) = -11.1$, $p = 3.76e\text{-}4$, Student's *t*-test).

SOX2-positive cells, constituting a part of Kölliker's organ cells and supporting cells within organs of Corti, also increased in number by 1.7 times in *Ebf1*$^{-/-}$ mice compared to *Ebf1*$^{+/+}$ mice (Fig. 5D, $t(6) = -16.5$, $p = 3.19e\text{-}6$, Student's *t*-test). PROX1-positive cell numbers significantly increased in *Ebf1*$^{-/-}$ mice compared to *Ebf1*$^{+/+}$ mice only in the basal and middle regions (Fig. 5E, $F(2, 18) = 91.41$, $p = 3.73e\text{-}10$, two-way ANOVA with Bonferroni *post-hoc* test). In the apical region, the number of PROX1-positive cells was similar to that in *Ebf1*$^{-/-}$ and *Ebf1*$^{+/+}$ mice. The numbers of PROX1-positive cells in *Ebf1*$^{+/+}$ and *Ebf1*$^{-/-}$ mice were 203.3 ± 2.2 and 439.0 ± 15.4, 228.0 ± 16.8 and 389.8 ± 10.4, and 196.0 ± 27.3 and 204.5 ± 19.6 in the basal, middle, and apical regions, respectively (Fig. 5*E*, basal: $p = 1.56e\text{-}13$; middle: $p = 8.99e\text{-}11$; apical; $p = 0.492$). When comparing the PROX1-positive cell numbers in the whole cochlea, the number was

significantly higher in *Ebf1*$^{-/-}$ mice (4980.7 ± 84.6) than *Ebf1*$^{+/+}$ mice (3769.7 ± 89.4) (Fig. 5F, $t(4) = -13.9$, $p = 1.54e\text{-}4$, Student's *t*-test).

We performed IHC analysis using more specific markers to reveal which population of hair or supporting cells increased in number in *Ebf1*$^{-/-}$ mice (Fig. 6). We immunostained whole-mounted cochlea at E18.5 with anti-VGLUT3 and anti-p75 (NGFR) antibodies, which indicate inner hair (Li et al., 2018) and pillar cells (von Bartheld et al., 1991), respectively. VGLUT3-positive inner hair cells, which are arranged in a single row in wild-type mice, were found to be increased in number in *Ebf1*$^{-/-}$ mice (Fig. 6A), indicating an increase in both inner and outer hair cells. The number of p75-positive pillar cells, which separate inner and outer hair cells, did not increase in *Ebf1*$^{-/-}$ mice (Fig. 6B). Considering that PROX1-positive cells indicate pillar and Deiters' cells, the number of Deiters' cells increased in *Ebf1*$^{-/-}$ mice. However, the arrangement of pillar cells was disrupted in *Ebf1*$^{-/-}$ mice (arrows in Fig. 6B), which was reflected in the appearance of VGLUT3 cells in the outer hair cell region of *Ebf1*$^{-/-}$ mice (arrowheads in Fig. 6A). In *Ebf1*$^{-/-}$ mice, the maturation markers, VGLUT3 and p75 were detected only in part of the cochlear regions. VGLUT3 was detected only in the basal region and p75 was in the basal and middle regions.

The total cochlear length, measured based on the length of the MYO7A-positive region (Fig. 7A), was slightly, but significantly, shorter in *Ebf1*$^{-/-}$ mice than in *Ebf1*$^{+/+}$ and *Ebf1*$^{+/-}$ mice (Fig. 7B, $F(2, 15) = 21.03$, $p = 4.44e\text{-}5$, one-way ANOVA with Tukey–Kramer *post-hoc* test, *Ebf1*$^{+/+}$ vs *Ebf1*$^{+/-}$: $p = 0.779$; *Ebf1*$^{+/+}$ vs *Ebf1*$^{-/-}$: $p = 2.74e\text{-}4$; *Ebf1*$^{+/-}$ vs *Ebf1*$^{-/-}$: $p = 7.80e\text{-}5$).

Ebf1 deletion caused the aberrant spiral ganglion and nerve fibers

As *Ebf1* is expressed in the spiral ganglion and the number of hair cells, a target of the spiral ganglion cell axon, increased in *Ebf1*$^{-/-}$ mice, we examined the spiral ganglion morphology and innervation of cochlear hair cells with IHC using anti-Tubulin β 3 (TUJ1) antibodies at E18.5 (Fig. 8).

Compared with *Ebf1*$^{+/+}$ mice, which exhibited axons extending from the spiral ganglion cells to the cochlear hair cells, *Ebf1*$^{-/-}$ mice had spiral ganglion cells (sg in Fig. 8A) under the organs of Corti (arrows in Fig. 8A), as well as in their normal position. The axons, which usually run parallel to the rows of outer hair cells, formed a reticulation within the *Ebf1*$^{-/-}$ mouse cochlear hair cell regions (Fig. 8B, C). Moreover, the innervation reached Kölliker's organ (arrowheads and brackets in Fig. 8A) as well as the organ of Corti.

Ebf1 deletion changed the distribution of JAG1-positive Kölliker's organ cells, the differentiation timing of a prosensory domain, and the proliferation of SOX2-positive cells

As *Ebf1*$^{-/-}$ mice had increased numbers of cochlear hair cells, which were differentiated from the prosensory domain, we investigated its specification, differentiation, proliferation, and cell death in the *Ebf1*$^{-/-}$ mouse cochlear duct floor.

First, to determine whether formation of the prosensory domain was affected by *Ebf1* deletion, we examined the formation of regions medial and lateral to the prosensory domain. Because these regions express FGF10 and BMP4 to induce non-sensory or sensory epithelia in the cochlear duct floor (Ohyama et al., 2010; Urness et al., 2015), respectively, we performed ISH for *Fgf10* and *Bmp4* in the basal region of the cochlear duct of *Ebf1*$^{+/+}$ *and Ebf1*$^{-/-}$ mice at E13.5 (Fig. 9A). The formation of both regions was similar in *Ebf1*$^{+/+}$ and *Ebf1*$^{-/-}$ mice, suggesting that *Ebf1* is not involved in the development of cell populations expressing *Fgf10* or *Bmp4*. To verify

468 the medial cell population more precisely, we immunostained E13.5 and E14.5 cochleae with an
469 anti-JAG1 antibody (Fig. 9A), as JAG1 is exclusively expressed in Kölliker's organ, a part of the
470 medial region, at this stage (Ohyama et al., 2010). JAG1-positive cells in *Ebf1*$^{-/-}$ mouse cochlea
471 expanded to the more medial region compared with those in *Ebf1*$^{+/+}$ mouse cochlea at E13.5 and
472 E14.5 (arrowheads in Fig. 9A).
473 Subsequently, we examined the expression of *Atoh1* within the prosensory domain via ISH at
474 E14.5 and E15.5 (Fig. 9B), as *Atoh1* is necessary for hair cells to differentiate from the
475 prosensory cell population (Bermingham et al., 1999) and its expression indicates the initiation
476 of hair cell development from the prosensory domain. Compared to *Ebf1*$^{+/+}$ mice that expressed
477 *Atoh1* within the prosensory domain from E14.5, *Atoh1* mRNA was not detected in the basal to
478 middle region of the E14.5 *Ebf1*$^{-/-}$ mouse cochlea, although the vestibular organs expressed
479 *Atoh1* within the prosensory epithelia. However, E15.5 *Ebf1*$^{-/-}$ mice exhibited an *Atoh1* signal
480 within the prosensory domain of the cochlea. This result suggests that while the cell fate
481 specification of sensory epithelia in the cochlea is not affected, its timing is delayed by *Ebf1*
482 deletion. Considering that the differentiation of cochlear sensory epithelia promotes the transition
483 from the basal to apical turns of the cochlea (Sher, 1971), the expression of hair and supporting
484 cell markers at a later stage, E18.5, also indicated delayed differentiation of *Ebf1*$^{-/-}$ mouse
485 cochleae (Fig. 6). These markers were found to be detected in more basal cochlear regions in
486 *Ebf1*$^{-/-}$ mice than in *Ebf1*$^{+/+}$ mice.
487 The expansion of the JAG1-positive cell area and the increased numbers of hair and supporting
488 cells suggest that the enhancement of proliferation or suppression of cell death occurs within the
489 prosensory domain and Kölliker's organ of *Ebf1*$^{-/-}$ mouse cochlea. To identify the mechanisms
490 that correlate with the functions of EBF1 within the cochlea, we tested the proliferation and

apoptotic status of *Ebf1*$^{-/-}$ mouse cochlea. To evaluate the proliferation status of the prosensory domain and Kölliker's organ, we immunostained cochlear sections with SOX2, a marker of the prosensory domain and a part of Kölliker's organ, and 5-ethynyl-2′-deoxyuridine (EdU) at E12.5, 13.5, 14.5, and 16.5 after administering EdU to pregnant mice (Fig. 10A). Quantification of SOX2-positive cells showed that their number decreased in *Ebf1*$^{+/+}$ mice from E12.5 onward (Fig. 10B), and their location was limited to the prosensory domain (brackets in Fig. 10A). In contrast, SOX2-positive cells in *Ebf1*$^{-/-}$ mouse cochlea were found both in the prosensory domain and the medial region, even at E13.5, which was consistent with the results of JAG1 immunostaining (Fig. 9A). The number of SOX2-positive cells in *Ebf1*$^{-/-}$ mice was similar to that in *Ebf1*$^{+/+}$ mice at E12.5, but increased at E13.5 and returned to the E12.5 level at E14.5 (Fig. 10B). Therefore, the number of SOX2-positive cells in *Ebf1*$^{-/-}$ mice was significantly higher than those in *Ebf1*$^{+/+}$ mice at E13.5 and E14.5 (Fig. 10B, $F(2, 18) = 12.61$, $p = 3.80\text{e-}4$, two-way ANOVA with Bonferroni *post-hoc* test; $p = 2.49\text{e-}4$ for E13.5 and $p = 1.36\text{e-}5$ for E14.5). The number of EdU-positive proliferating cells within SOX2-positive cells was significantly higher in *Ebf1*$^{-/-}$ mice than in *Ebf1*$^{+/+}$ mice at E13.5 and E14.5 (Fig. 10C, $F(2, 18) = 10.61$, $p = 9.50\text{e-}4$, two-way ANOVA with Bonferroni post-hoc test; $p = 9.55\text{e-}6$ for E13.5 and $p = 1.00\text{e-}3$ for E14.5). As the number of SOX2-positive cells increased in *Ebf1*$^{-/-}$ mice after E13.5 (Fig. 10B), normalization of SOX2-positive cell numbers was necessary to correctly evaluate the proliferation status of SOX2-positive cells. We calculated the proportion of EdU-positive cells among SOX2-positive cells and found that the proliferation was enhanced in the SOX2-positive cells of *Ebf1*$^{-/-}$ mouse cochlea only at E13.5 (49.8 ± 4.3%) compared with that in *Ebf1*$^{+/+}$ mouse cochlea (37.8 ± 4.2%) (Fig. 10D, $F(2, 18) = 5.84$, $p = 0.011$, two-way ANOVA with Bonferroni *post-hoc* test; $p = 9.45\text{e-}4$ for E13.5). These results suggested that EBF1 suppressed the

514 proliferation of SOX2-positive cells within a limited time window. Morphologically, a difference
515 in proliferation was observed in the prosensory domain, as indicated by EdU immunostaining
516 (brackets at E13.5; Fig. 10A). EdU staining was observed in the Kölliker's organs of *Ebf1*$^{-/-}$ mice,
517 even at E16.5 (arrowhead in Fig. 10A), but not observed in *Ebf1*$^{+/+}$ mice (E16.5 of Fig. 10A).
518 The loss of proliferation within the prosensory domain around E13.5 (bracket in the *Ebf1*$^{+/+}$
519 sample at E13.5, Fig. 10A) has been well documented in previous studies (Chen and Segil, 1999;
520 Chen et al., 2002). The post-mitotic domain is called the zone of non-proliferating cells (ZNPC),
521 and is characterized by the expression of the cyclin-dependent kinase inhibitor CDKN1B. To
522 confirm the EdU immunostaining results, we performed CDKN1B immunostaining at E13.5 and
523 E14.5 (Fig. 10E). Although CDKN1B was detected in the prosensory domain of *Ebf1*$^{+/+}$ mice at
524 E13.5, it was not expressed in *Ebf1*$^{-/-}$ mouse cochlea at this stage (arrows in Fig. 10E), which was
525 consistent with the results of EdU detection. At E14.5, CDKN1B was detected in a larger area of
526 the middle part of *Ebf1*$^{-/-}$ mouse cochlear duct floors than in those of *Ebf1*$^{+/+}$ mice. To quantify
527 the change of the CDKN1B immunostaining, we counted the number of CDKN1B- and SOX2-
528 double-positive cells at E13.5 and E14.5 (Fig. 10*F*). We found that *Ebf1* deletion resulted in
529 significant loss of CDKN1B- and SOX2- double-positive cells at E13.5 (79.0 ± 3.7; *Ebf1*$^{+/+}$ vs
530 2.6 ± 2.1; *Ebf1*$^{-/-}$, $t(4) = 25.3$, $p = 1.45e\text{-}5$, Student's *t*-test). In contrast, the number in *Ebf1*$^{-/-}$
531 mice was almost twice as high as that in *Ebf1*$^{+/+}$ mice at E14.5 (43.3 ± 8.7; *Ebf1*$^{+/+}$ vs 87.3 ± 4.8;
532 *Ebf1*$^{-/-}$, $t(6) = -7.68$, $p = 2.54e\text{-}4$, Student's *t*-test). Apoptosis within the inner ear or cochlear duct
533 did not increase in *Ebf1*$^{-/-}$ mice at E11.5 and E13.5, compared with that in *Ebf1*$^{+/+}$ mice (Fig. 11).
534
535 **Ebf1 deletion impairs auditory function**

536 The aberrant cochlear sensory epithelia observed in *Ebf1*-deleted mice suggest that hearing
537 ability is impaired in these mice. To evaluate the effect of *Ebf1* deletion on auditory function, we
538 measured the ABR (Fig. 12A) and DPOAE (Fig. 12B) in P21 *Foxg1Cre;Ebf1*$^{fl/fl}$ mice. We did
539 not use *Ebf1*$^{-/-}$ mice for this analysis to avoid embryonic lethality and to eliminate the effects of
540 the hypoplastic scala tympani observed in *Ebf1*$^{-/-}$mice on auditory function. The phenotype of
541 *Foxg1Cre;Ebf1*$^{fl/fl}$ mice was evaluated using whole-mount cochlear samples collected at P23 (Fig.
542 12C). We observed a marked increase in the number of cochlear hair cells in *Foxg1Cre;Ebf1*$^{fl/fl}$
543 mice, comparable to the morphology of E18.5 *Ebf1*$^{-/-}$ and *Foxg1Cre;Ebf1*$^{fl/fl}$ mice (Fig. 4B and
544 Fig. 12C).
545 ABR measurement showed significant elevations of thresholds of the response to sound in
546 *Foxg1Cre;Ebf1*$^{fl/fl}$ mice at all frequencies examined (10 kHz, 93.3 ± 2.5 dB; 20 kHz, 86.7 ± 3.8
547 dB; 40 kHz, 105.0 ± 0.0 dB) (Fig. 12A, $F(2, 12) = 5.21$, $p = 0.023$, two-way ANOVA with
548 Bonferroni *post-hoc* test) compared with control mice, indicating severe hearing loss in *Ebf1*-
549 deleted mice. Subsequently, we performed DPOAE tests to assess the function of the increased
550 number of outer hair cells caused by *Ebf1* deletion because DPOAE detects nonlinear responses
551 of outer hair cells to sound. The DPOAE responses in *Foxg1Cre;Ebf1*$^{fl/fl}$ mice were significantly
552 lower than those in control mice (Fig. 12B, $F(7, 48) = 5.54$, $p = 1.03\text{e-}4$, two-way ANOVA with
553 Bonferroni *post-hoc* test). The decreased DPOAE response in *Foxg1Cre;Ebf1*$^{fl/fl}$ mice also
554 suggests that the increased number of hair cells caused by *Ebf1* deletion did not function as outer
555 hair cells.
556
557 **Discussion**
558 The results of this study indicate a novel and interesting role of *Ebf1* in the cochlear

559 development. *Ebf1* controls numbers of both hair and supporting cells within the cochlear
560 sensory epithelia. Moreover, *Ebf1* is important for the development of the scala tympani, spiral
561 limbus, and spiral ganglion cells.
562 Since EBF1 was originally identified from the regulators of early B cell differentiation (Hagman
563 et al., 1991) and olfactory-specific genes (Wang and Reed, 1993), its expression has been
564 reported in all three germinal layers (Liberg et al., 2002). EBF1 has many roles, including cell
565 fate specification, the differentiation, maturation, and migration of cells, and path findings by
566 neurons (Liberg et al., 2002).
567 The present study revealed that *Ebf1* is expressed in ectodermal tissues (the inner ear epithelium
568 and spiral ganglion) and the otic mesenchymal tissues. Its expression in the inner ear began at
569 approximately E10.5, as confirmed by qRT-PCR and ISH (Fig. 1A and C). Within the cochlea,
570 *Ebf1* expression in the cochlea was not limited to the *Sox2*-positive prosensory domain (white
571 arrows in Fig. 1B) but expanded toward a more medial region in the cochlear duct floor, where
572 Kölliker's organ exists (Fig. 1B, C and Fig. 2A). Thus, the *Ebf1* expression area comprised most
573 of the GER.
574 To elucidate the function of *Ebf1* in inner ear development, we examined the inner ear
575 morphology of *Ebf1* conventional ($Ebf1^{-/-}$) and inner ear epithelia-specific conditional
576 ($Foxg1Cre;Ebf1^{fl/fl}$) knockout mice. In contrast to the normal vestibular morphology of $Ebf1^{-/-}$
577 mice, the cochlea of *Ebf1*-deleted mice showed various phenotypes, indicating that other *Ebf*
578 subtypes do not have redundant functions with *Ebf1* in the cochlea as in B cells, osteoblasts, and
579 the striatum (Lin and Grosschedl, 1995; Garel et al., 1999; Nieminen-Pihala et al., 2021). HE
580 staining revealed loss of the scala tympani and spiral limbus in $Ebf1^{-/-}$ mice (Fig. 3C). Because
581 both structures are derived from mesenchymal tissues (Sher, 1971; Phippard et al., 1999), we

582 hypothesized that these phenotypes reflect the roles of EBF1 in cochlear mesenchyme. To
583 confirm this, we compared the formation of the scala tympani and spiral limbus between *Ebf1*$^{-/-}$
584 and *Foxg1Cre;Ebf1*$^{fl/fl}$ mice (Fig. 3C). Although the scala tympani developed normally in
585 *Foxg1Cre;Ebf1*$^{fl/fl}$ mice, the spiral limbus was hypoplastic in both *Foxg1Cre;Ebf1*$^{fl/fl}$ and *Ebf1*$^{-/-}$
586 mice. These results clearly indicate that EBF1 in the cochlear epithelia is not required in the
587 formation of the scala tympani as suggested by previous reports. In contrast, spiral limbus
588 formation depends on epithelial expression of *Ebf1*, which is surprising. Mesenchyme-specific
589 deletion of *Ebf1* will elucidate how EBF1 forms the spiral limbus. The shorter cochlear duct in
590 *Ebf1*$^{-/-}$ mice than in *Foxg1Cre;Ebf1*$^{fl/fl}$ mice suggests that epithelial EBF1 is not involved in
591 regulating the length of the cochlear duct as well.
592 More prominent roles of *Ebf1* have been found in the cochlear epithelia. By deleting *Ebf1*, the
593 numbers of both hair and supporting cells increased at E18.5 (Fig. 4 and 5). We observed an
594 increase in the numbers of both inner and outer hair cells (Fig. 6). This phenotype suggests that
595 EBF1 is involved in the regulation of hair and supporting cell number during cochlear
596 development. To determine its mechanisms, we evaluated the specifications and differentiation
597 of the cochlear prosensory domain and its proliferation and cell death status under *Ebf1* knockout
598 conditions. We found that the formation of cochlear non-sensory regions medial and lateral to
599 the prosensory domain were normal in *Ebf1*$^{-/-}$ mice (Fig. 9A), indicating that the phenotypes of
600 *Ebf1*$^{-/-}$ mouse cochlear sensory epithelia were caused by factors within the prosensory domain. In
601 contrast to markers outside the prosensory domain, the molecules expressed in the prosensory
602 domain and Kölliker's organs, JAG1 and SOX2, showed abnormal expression patterns (Fig. 2,
603 Fig. 4A, and Fig. 9A). These two molecules were expressed in a more medial region of the *Ebf1*$^{-}$
604 $^{/-}$ mouse cochlear duct floor at E14.5 and E18.5. The fact that EBF1 was expressed in a more

605 medial region than SOX2 in wild-type mice indicates that it plays a role in suppressing the
606 localization of JAG1- and SOX2-positive cells in the most medial region. The study of
607 proliferation status within the SOX2-positive cells showed that *Ebf1* deletion enhanced the
608 proliferation of SOX2-positive cells specifically at E13.5 (Fig. 10 D), which was supported by
609 the loss of CDKN1B expression in the possible prosensory domain of the *Ebf1*$^{-/-}$ mice at E13.5
610 (Fig. 10E, F). The highest *Ebf1* expression level at E13.5 (Fig. 1A) may be related to these
611 phenotypes in *Ebf1*$^{-/-}$ mice. This aberrant proliferation within SOX2-positive cells was suggested
612 to increase the numbers of hair and supporting cells at later stages (Fig. 4A, B, and D).
613 Evaluation of hearing ability at the postnatal stage showed that an increase in hair and supporting
614 cell numbers resulted in an increased hearing threshold (Fig. 12). These results indicate that
615 EBF1 suppresses the proliferation of SOX2-positive cells and thus contributes to the
616 development of appropriate numbers of hair and supporting cells, resulting in the development of
617 normal auditory function. Rich expression of EBF1 in SOX2-positive cells within the medial part
618 of the cochlear duct floor, containing the Kölliker's organ (Kolla et al., 2020) and the GER
619 (Kubota et al., 2021), suggests that these regions are involved in the regulation of the hair and
620 supporting cell number. Several lines of evidence support the function of EBF1 to suppress cell
621 proliferation. Human EBF1 has been reported to suppress the proliferation of malignant tumors
622 (Shen et al., 2020), and the deletion of *Rb1*, a known tumor suppressor and cell cycle regulator
623 (Lipinski and Jacks, 1999; Classon and Harlow, 2002), results in the same morphology in the
624 cochlea as that caused by *Ebf1* deletion (Sage et al., 2005). The gain-of-function study will
625 confirm that the regulation of the proliferation is the primary role of EBF1 in the cochlea.
626 The expression of mature cochlear cell markers, including MYO7A, VGULT3, and p75, in *Ebf1*$^{-}$
627 $^{/-}$ mice indicated that each cell type developed with normal cell fate specification. Although some

GER cells in the *Ebf1*-deleted mouse cochlea ectopically expressed the hair cell marker MYO7A (Fig. 4B and C), the penetrance of this phenotype was low. Cell fate may be regulated by EBF1 in the cochlea to a small extent; however, cell specification is not a prominent role of cochlear EBF1, which is different from B lymphocytes (Nechanitzky et al., 2013). In contrast, several results from our study indicate that the differentiation appears to delay in the *Ebf1*$^{-/-}$ mouse cochlea. The expression of *Atoh1* within the cochlear prosensory domain, which was observed at E14.5 in wild-type mice, was detected as late as E15.5 in *Ebf1*$^{-/-}$ mice (Fig. 9B). VGLUT3- and p75-positive cells were not detected in the apical region in *Ebf1*$^{-/-}$ mouse cochlea at E18.5 (Fig. 6). This delay in differentiation may be caused by the aberrant proliferation of the prosensory domain in *Ebf1*$^{-/-}$ mice, as the deterioration of proliferation affects the differentiation of cochlear hair cells (Bok et al., 2013; Golden et al., 2015).

An altered neuroaxonal composition of spiral ganglion neuronal cells in the *Ebf1*-deleted organ of Corti (Fig. 8) suggests that EBF1 may affect the pathfinding of spiral ganglion cells within the cochlea, as observed in facial branchiomotor neurons and retina (Garel et al., 2000; Jin and Xiang, 2011). Considering the role of otic mesenchyme in the innervation of spiral ganglion axons on hair cells (Coate and Kelley, 2013), mesenchymal *Ebf1* defect may also contribute to the phenotype observed in the spiral ganglion cells.

The *Ebf1* is expressed in the medial region of the cochlear duct floor (Fig. 1B, C, and Fig. 2) and the spiral limbus loss (Fig. 3C) and ectopic MYO7A-positive cells within the GER (Fig. 4B and C) in *Ebf1*-deleted mice are similar to the phenotype of knockout mice of *Prdm16*, a marker of Kölliker's organ. Moreover, *Prdm16* knockout mice showed decreased expression of *Ebf1* in the cochlear duct (Ebeid et al., 2022). These support the involvement of EBF1 in the Kölliker's organ development.

651 The phenotypes of the increased numbers of hair and supporting cells suggest the involvement
652 of molecules crucial for the development of cochlear sensory epithelia, including Notch signal-
653 related molecules (Yamamoto et al., 2011) and SOX2 (Kiernan et al., 2005), in the regulation of
654 *Ebf1* expression. However, that is not a case because *Ebf1*-expression levels did not change in
655 striatal neurons of *Foxg1Cre*-mediated *Notch 1*- or *Sox2*-deleted mice (Mason et al., 2005; Ferri
656 et al., 2013). Identification of the molecules upstream and downstream of EBF1 will be the next
657 step in revealing the precise function of EBF1 in the cochlea and the grand scheme of inner ear
658 development.
659 In conclusion, *Ebf1* and its protein are expressed in the epithelia of the inner ear prosensory
660 domain as well as in Kölliker's organ, the mesenchyme, and CVG cells within the cochlea, and
661 play important roles in the formation of each structure. Epithelial EBF1 regulates the number of
662 cochlear hair and supporting cells by suppressing the proliferation of the prosensory domain and
663 Kölliker's organ cells, mainly at E13.5. Therefore, epithelial EBF1 is crucial for normal hearing
664 in mammals.
665

666 **References**

667 Bermingham-McDonogh O, Oesterle EC, Stone JS, Hume CR, Huynh HM, Hayashi T (2006)
668 Expression of Prox1 during mouse cochlear development. The Journal of comparative
669 neurology 496:172-186.
670 Bermingham NA, Hassan BA, Price SD, Vollrath MA, Ben-Arie N, Eatock RA, Bellen HJ,
671 Lysakowski A, Zoghbi HY (1999) Math1: an essential gene for the generation of inner
672 ear hair cells. Science 284:1837-1841.
673 Bok J, Zenczak C, Hwang CH, Wu DK (2013) Auditory ganglion source of Sonic hedgehog
674 regulates timing of cell cycle exit and differentiation of mammalian cochlear hair cells.
675 Proc Natl Acad Sci U S A 110:13869-13874.
676 Chen P, Segil N (1999) p27(Kip1) links cell proliferation to morphogenesis in the developing
677 organ of Corti. Development 126:1581-1590.
678 Chen P, Johnson JE, Zoghbi HY, Segil N (2002) The role of Math1 in inner ear development:
679 Uncoupling the establishment of the sensory primordium from hair cell fate
680 determination. Development 129:2495-2505.

Classon M, Harlow E (2002) The retinoblastoma tumour suppressor in development and cancer. Nature Reviews Cancer 2:910-917.
Coate TM, Kelley MW (2013) Making connections in the inner ear: Recent insights into the development of spiral ganglion neurons and their connectivity with sensory hair cells. Seminars in Cell and Developmental Biology 24:460-469.
Dayaratne MW, Vlajkovic SM, Lipski J, Thorne PR (2014) Kolliker's organ and the development of spontaneous activity in the auditory system: implications for hearing dysfunction. BioMed research international 2014:367939.
Ebeid M, Barnas K, Zhang H, Yaghmour A, Noreikaite G, Bjork BC (2022) PRDM16 expression and function in mammalian cochlear development. Developmental Dynamics.
Ferri A, Favaro R, Beccari L, Bertolini J, Mercurio S, Nieto-Lopez F, Verzeroli C, La Regina F, De Pietri Tonelli D, Ottolenghi S, Bovolenta P, Nicolis SK (2013) Sox2 is required for embryonic development of the ventral telencephalon through the activation of the ventral determinants Nkx2.1 and Shh. Development 140:1250-1261.
Garel S, Garcia-Dominguez M, Charnay P (2000) Control of the migratory pathway of facial branchiomotor neurones. Development 127:5297-5307.
Garel S, Marin F, Grosschedl R, Charnay P (1999) Ebf1 controls early cell differentiation in the embryonic striatum. Development 126:5285-5294.
Golden EJ, Benito-Gonzalez A, Doetzlhofer A (2015) The RNA-binding protein LIN28B regulates developmental timing in the mammalian cochlea. Proc Natl Acad Sci U S A 112:E3864-3873.
Gyory I, Boller S, Nechanitzky R, Mandel E, Pott S, Liu E, Grosschedl R (2012) Transcription factor Ebf1 regulates differentiation stage-specific signaling, proliferation, and survival of B cells. Genes and Development 26:668-682.
Hagman J, Travis A, Grosschedl R (1991) A novel lineage-specific nuclear factor regulates mb-1 gene transcription at the early stages of B cell differentiation. The EMBO journal 10:3409-3417.
Hagman J, Gutch MJ, Lin H, Grosschedl R (1995) EBF contains a novel zinc coordination motif and multiple dimerization and transcriptional activation domains. EMBO Journal 14:2907-2916.
Hamaguchi K, Yamamoto N, Nakagawa T, Furuyashiki T, Narumiya S, Ito J (2012) Role of PGE-type receptor 4 in auditory function and noise-induced hearing loss in mice. Neuropharmacology 62:1841-1847.
Hébert JM, McConnell SK (2000) Targeting of cre to the Foxg1 (BF-1) locus mediates loxP recombination in the telencephalon and other developing head structures. Developmental Biology 222:296-306.
Jin K, Xiang M (2011) Ebf1 deficiency causes increase of Müller cells in the retina and abnormal topographic projection at the optic chiasm. Biochemical and Biophysical Research Communications 414:539-544.
Kada S, Nakagawa T, Ito J (2009) A Mouse Model for Degeneration of the Spiral Ligament. Journal of the Association for Research in Otolaryngology 10:161-172.
Kiernan AE, Pelling AL, Leung KKH, Tang ASP, Bell DM, Tease C, Lovell-Badge R, Steel KP, Cheah KSE (2005) Sox2 is required for sensory organ development in the mammalian inner ear. Nature 434:1031-1035.
Kolla L, Kelly MC, Mann ZF, Anaya-Rocha A, Ellis K, Lemons A, Palermo AT, So KS, Mays JC, Orvis J, Burns JC, Hertzano R, Driver EC, Kelley MW (2020) Characterization of the

development of the mouse cochlear epithelium at the single cell level. Nature communications 11:2389.
Kubota M, Scheibinger M, Jan TA, Heller S (2021) Greater epithelial ridge cells are the principal organoid-forming progenitors of the mouse cochlea. Cell Reports 34:108646.
Li C, Shu Y, Wang G, Zhang H, Lu Y, Li X, Li G, Song L, Liu Z (2018) Characterizing a novel vGlut3-P2A-iCreER knockin mouse strain in cochlea. Hear Res 364:12-24.
Liberg D, Sigvardsson M, Akerblad P (2002) The EBF/Olf/Collier family of transcription factors: regulators of differentiation in cells originating from all three embryonal germ layers. Molecular and Cellular Biology 22:8389-8397.
Lin H, Grosschedl R (1995) Failure of B-cell differentiation in mice lacking the transcription factor EBF. Nature 376:263-267.
Lipinski MM, Jacks T (1999) The retinoblastoma gene family in differentiation and development. Oncogene 18:7873-7882.
Mason HA, Rakowiecki SM, Raftopoulou M, Nery S, Huang Y, Gridley T, Fishell G (2005) Notch signaling coordinates the patterning of striatal compartments. Development 132:4247-4258.
Nechanitzky R, Akbas D, Scherer S, Gyory I, Hoyler T, Ramamoorthy S, Diefenbach A, Grosschedl R (2013) Transcription factor EBF1 is essential for the maintenance of B cell identity and prevention of alternative fates in committed cells. Nature immunology 14:867-875.
Nieminen-Pihala V, Tarkkonen K, Laine J, Rummukainen P, Saastamoinen L, Nagano K, Baron R, Kiviranta R (2021) Early B-cell Factor1 (Ebf1) promotes early osteoblast differentiation but suppresses osteoblast function. Bone 146:115884.
Ohyama T, Basch ML, Mishina Y, Lyons KM, Segil N, Groves AK (2010) BMP Signaling Is Necessary for Patterning the Sensory and Nonsensory Regions of the Developing Mammalian Cochlea. Journal of Neuroscience 30:15044-15051.
Phippard D, Lu L, Lee D, Saunders JC, Crenshaw EB, 3rd (1999) Targeted mutagenesis of the POU-domain gene Brn4/Pou3f4 causes developmental defects in the inner ear. The Journal of neuroscience : the official journal of the Society for Neuroscience 19:5980-5989.
Sage C, Huang M, Karimi K, Gutierrez G, Vollrath MA, Zhang DS, Garcia-Anoveros J, Hinds PW, Corwin JT, Corey DP, Chen ZY (2005) Proliferation of functional hair cells in vivo in the absence of the retinoblastoma protein. Science 307:1114-1118.
Saino-Saito S, Suzuki R, Tokuda N, Abe H, Kondo H, Owada Y (2010) Localization of fatty acid binding proteins (FABPs) in the cochlea of mice. Ann Anat 192:210-214.
Schneider CA, Rasband WS, Eliceiri KW (2012) NIH Image to ImageJ: 25 years of image analysis. Nat Methods 9:671-675.
Shen Z, Chen Y, Li L, Liu L, Peng M, Chen X, Wu X, Sferra TJ, Wu M, Lin X, Cheng Y, Chu J, Shen A, Peng J (2020) Transcription Factor EBF1 Over-Expression Suppresses Tumor Growth in vivo and in vitro via Modulation of the PNO1/p53 Pathway in Colorectal Cancer. Front Oncol 10:1035.
Sher AE (1971) The embryonic and postnatal development of the inner ear of the mouse. Acta oto-laryngologica Supplementum 285:1-77.
Taniguchi M, Yamamoto N, Nakagawa T, Ogino E, Ito J (2012) Identification of tympanic border cells as slow-cycling cells in the cochlea. PloS one 7:e48544.

Urness LD, Wang X, Shibata S, Ohyama T, Mansour SL (2015) Fgf10 is required for specification of non-sensory regions of the cochlear epithelium. Developmental Biology 400:59-71.
von Bartheld CS, Patterson SL, Heuer JG, Wheeler EF, Bothwell M, Rubel EW (1991) Expression of nerve growth factor (NGF) receptors in the developing inner ear of chick and rat. Development 113:455-470.
Wang MM, Reed RR (1993) Molecular cloning of the olfactory neuronal transcription factor Olf-1 by genetic selection in yeast. Nature 364:121-126.
Wu DK, Kelley MW (2012) Molecular mechanisms of inner ear development. Cold Spring Harbor Perspectives in Biology 4:a008409.
Yamamoto N, Chang W, Kelley MW (2011) Rbpj regulates development of prosensory cells in the mammalian inner ear. Developmental Biology 353:367-379.
Yamamoto R, Ohnishi H, Omori K, Yamamoto N (2021) In silico analysis of inner ear development using public whole embryonic body single-cell RNA-sequencing data. Developmental Biology 469:160-171.

Figures and Figure Legends

Figure 1. Quantitative and spatiotemporal expression of *Ebf1* during inner ear development.

A. Results of quantitative reverse transcription polymerase chain reaction (qRT-PCR) analysis for *Ebf1* in the inner ear of wild-type mice from embryonic day (E) 9.5 to postnatal day (P) 0. The value of each date is normalized to the value of E9.5. Box plot representing the medians and interquartile ranges of the relative mRNA expression of *Ebf1* (n = 3). **B** and **C**. Result of *in situ* hybridization for *Ebf1* and *Sox2* in cross sections of the inner ear of wild-type mice at E13.5 (B) and E9.5, E10.5, E11.5, E12.5, E16.5, E18.5, and P0 (C). Areas enclosed by dashed lines indicate the inner ear epithelium. Low-magnification images of the cochlear basal turn and vestibule are presented in the uppermost panels of **B**. High-magnification images of the apical turn of the cochlear duct and vestibules are presented in the middle and lower panels of **B**, respectively. Images of E9.5 and E10.5 otocysts and E11.5, E12.5, E16.5, E18.5, and P0 cochleae and vestibules are presented in the uppermost, middle, and lowermost images of **C**, respectively. From E11.5 to P0, Ebf1 is expressed in the sensory epithelium of the cochlea (white arrows or Ko and oC), the vestibular and semicircular canals (black arrows), the spiral ganglion (white asterisks), and the surrounding mesenchymal tissues (black asterisks and SL) . The expression is detected in tympani border cells (white arrowhead). One-way analysis of variance (ANOVA) with Tukey–Kramer *post-hoc* tests was performed. *p <0.05, **p <0.01. D, dorsal; L, lateral. cd, cochlear duct; sg, spiral ganglion; Ut, utricle; Sa, saccule; Lc, lateral crista; SL, spiral ligament; Ko, Kölliker's organ; oC, organ of Corti. Scale bars: 100 μm.

Figure 2. Expression of EBF1 in the cochlea of wild type and *Ebf1*-deleted mice

A. Immunohistochemical images of E14.5 *Ebf1*$^{+/+}$ (upper panels) and *Ebf1*$^{-/-}$ (lower panels) mouse cochlear ducts labeled with EBF1 (green) and SOX2 (magenta). **B.** Immunohistochemical images of E13.5 (left panels) and E18.5 (right panels) *Foxg1Cre;Ebf1*$^{fl/+}$ (Cre;EBF1$^{fl/+}$) (upper panels) and *Foxg1Cre;Ebf1*$^{fl/fl}$ (Cre;EBF1$^{fl/fl}$) (lower panels) mouse cochlear ducts labeled with EBF1 (green) and SOX2 (magenta). EBF1 is expressed throughout Kölliker's organ and the prosensory domain, whereas SOX2 was expressed in a part of Kölliker's organ and the prosensory domain as well as otic mesenchyme in wild type mouse cochlea. The signal for EBF1 is absent in the cochlear epithelium and otic mesenchyme in *Ebf1*$^{-/-}$ mouse and in the cochlear epithelium in *Foxg1Cre;Ebf1*$^{fl/fl}$ mice. The EBF1 signal is observed in the otic mesenchyme of *Foxg1Cre;Ebf1*$^{fl/fl}$ mice (arrows in **B**). SOX2 is expressed in the medial region of *Ebf1*$^{-/-}$ mice cochlear duct floor (arrowhead in **A**). Areas enclosed by dashed lines indicate the cochlear epithelium. Ko, Kölliker's organ; Pd, prosensory domain. Scale bars: 100 μm.

Figure 3. Development of the cochlear duct is deteriorated in *Ebf1*-deleted mice.

A. Gross morphology of membranous labyrinth of the inner ear of *Ebf1*$^{+/+}$ and *Ebf1*$^{-/-}$mice at embryonic day (E) 18.5. **B.** Gross morphology of the cochlear duct floor after the lateral wall and Reissner's membrane of the cochlea were removed at E18.5. **C.** Hematoxylin and eosin-stained cross sections of the cochlea at E18.5 from *Ebf1*$^{+/+}$, *Ebf1*$^{-/-}$, *Foxg1Cre;Ebf1*$^{fl/+}$ (Cre;EBF1$^{fl/+}$), and *Foxg1Cre;Ebf1*$^{fl/fl}$ (Cre;EBF1$^{fl/fl}$) mice. Images in dashed boxes in the uppermost row were magnified into the second row (from boxes labeled as b in the uppermost row, a basal turn) and the third row (from boxes labeled as m in the uppermost row, a middle turn). The images in the lowermost row are the magnified images of the third row (middle turn). Areas enclosed by dashed lines indicate the spiral limbus. **D.** Immunohistochemical images of the basal turn of the

Ebf1$^{+/+}$, *Ebf1*$^{-/-}$, *Foxg1Cre;Ebf1*$^{fl/+}$, and *Foxg1Cre;Ebf1*$^{fl/fl}$ mice cochlear ducts at E18.5, labeled with MYO7A (gray) and FABP7 (green). Areas enclosed by dashed lines indicate the spiral limbus. **E.** Areas of spiral limbus in the basal and middle region of the cochlear ducts of *Ebf1*$^{+/+}$, *Ebf1*$^{-/-}$, *Foxg1Cre;Ebf1*$^{fl/+}$, and *Foxg1Cre;Ebf1*$^{fl/fl}$ mice at E18.5. Student's *t*-test was performed for comparison between *Ebf1*-deleted mice (*Ebf1*$^{-/-}$ or *Foxg1Cre;Ebf1*$^{fl/fl}$) and respective controls (*Ebf1*$^{+/+}$ or *Foxg1Cre;Ebf1*$^{fl/+}$). **p* <0.001, ***p* <0.0001. Error bars represent mean ± standard deviation (n = 4). cd, cochlear duct; Ut, utricle; Sa, saccule; Lc, lateral crista; Pc, posterior crista; b, basal turn; m, middle turn; sv, scala vestibuli; sm, scala media; st, scala tympani; sl, spiral limbus: Ko, Kölliker's organ; oC, organ of Corti. Scale bars: 0.5 mm in **A** and **B** and 100 μm in **C** and **D**.

Figure 4. *Ebf1* deletion increases the number of MYO7A-, SOX2-, and PROX1-positive cells in the cochlea.

A. Cross sections of the basal and apical turns of the cochlea of *Ebf1*$^{+/+}$, *Ebf1*$^{-/-}$, *Foxg1Cre;Ebf1*$^{fl/+}$ (Cre;EBF1$^{fl/+}$), and *Foxg1Cre;Ebf1*$^{fl/fl}$ (Cre;EBF1$^{fl/fl}$) mice at embryonic day (E) 18.5, labeled with MYO7A (green) and SOX2 (magenta). Magnified images of the organ of Corti (oC) and Kölliker's organ (Ko) are presented in the eight right panels. **B**. Whole mount cochlear images from *Ebf1*$^{+/+}$, *Ebf1*$^{-/-}$, *Foxg1Cre;Ebf1*$^{fl/+}$ (Cre;EBF1$^{fl/+}$), and *Foxg1Cre;Ebf1*$^{fl/fl}$ (Cre;EBF1$^{fl/fl}$) mice, labeled with MYO7A (green) and SOX2 (magenta). **C** and **D**. Whole mount cochlear images from *Ebf1*$^{+/+}$ and *Ebf1*$^{-/-}$ mice at E18.5, labeled with MYO7A (green, **C**), phalloidin (white, **C**), and PROX1 (green, **D**). Scale bars: 50 μm in **A**, **B**, and **D**; 10 μm in **C**.

Figure 5. Increases in the number of hair and supporting cells.

A. Schematic diagram of the cochlea duct showing the positions of the basal, middle, and apical regions of the cochlea. **B**. Total hair cell numbers per 200 μm in the basal, middle, and apical regions of the cochlear ducts of *Ebf1*$^{+/+}$, *Ebf1*$^{+/-}$, and *Ebf1*$^{-/-}$ mice at embryonic day (E) 18.5. **C**. Numbers of MYO7A-positive cells per total cochlear length. **D**. Numbers of SOX2-positive cells per 100 μm in the basal region of the cochlea. **E**. Numbers of PROX1-positive cells per 200 μm in the basal, middle, and apical regions of the cochlea. **F.** Numbers of PROX1-positive cells per total cochlear length. Two-way ANOVA with Bonferroni *post-hoc* test (**B** and **E**) and Student's *t*-test (**C, D** and **F**) were performed. *$p < 0.05$, **$p < 0.01$, ***$p < 0.001$, and ****$p < 0.0001$; ns, not significant. Error bars represent mean ± standard deviation (n = 4 for **B**, **D**, **E**, and n = 3 for **C**, **F**).

Figure 6. *Ebf1* deletion causes increased number of inner hair cells and delayed differentiation of hair and supporting cells.

High-magnification images of the basal, middle, and apical regions of whole-mount cochlear samples from E18.5 *Ebf1*$^{+/+}$ and *Ebf1*$^{-/-}$ mice. **A**. Immunostaining with phalloidin (green) and an anti-VGLUT3 antibody (magenta). In the cochlea of *Ebf1*$^{-/-}$ mice, the row number of VGLUT3-positive cells was 2 to 3, whereas this number was only 1 in wild-type mice. VGLUT3-positive cells were observed only in the basal region of the cochlea but not in the middle and apical regions of *Ebf1*$^{-/-}$ mice. Several VGLUT3-positive cells were observed in the outer hair cell area (arrowheads). **B**. Immunostaining with anti-MYO7A (gray) and p75 (green) antibodies. In the cochlea of *Ebf1*$^{-/-}$ mice, the row number of p75-positive cells was similar to that in *Ebf1*$^{+/+}$ mice, although their arrangement was deteriorated in *Ebf1*$^{-/-}$ mice (arrow**)**. p75-positive cells are observed only in the basal and middle region in the *Ebf1*$^{-/-}$ mice. Scale bars: 20 μm.

881

882 **Figure 7. Quantification of cochlear length.**

883 **A**. Whole mount images of the cochlea of embryonic day (E) 18.5 *Ebf1*$^{+/+}$, *Ebf1*$^{+/-}$, and *Ebf1*$^{-/-}$
884 mice labeled with MYO7A (green). **B**. Quantification of cochlear duct length of E18.5 *Ebf1*$^{+/+}$,
885 *Ebf1*$^{+/-}$, and *Ebf1*$^{-/-}$ mice. The cochlear length of *Ebf1*$^{-/-}$ mice was significantly shorter than those
886 of *Ebf1*$^{+/+}$and *Ebf1*$^{+/-}$ mice. Two-way ANOVA with Bonferroni *post-hoc* test was performed. **p*
887 < 0.001, and ***p* < 0.0001; ns, not significant. Error bars represent mean ± standard deviation (n
888 = 6). Scale bar: 200 μm.

889

890 **Figure 8. *Ebf1* deletion causes aberrant spiral ganglion development and axon outgrowth to**
891 **cochlear hair cells.**

892 **A**. Cross sections of the basal, middle, and apical regions of the cochlea and spiral ganglion in
893 embryonic day (E) 18.5 *Ebf1*$^{+/+}$ and *Ebf1*$^{-/-}$ mice stained with Tubulin β 3 (TUJ1, green) and
894 4',6-diamidino-2-phenylindole (DAPI, gray). The morphology of the spiral ganglion in *Ebf1*$^{-/-}$
895 mice differed from that in *Ebf1*$^{+/+}$ mice. TUJ1-positive cell bodies were observed below the
896 organ of Corti (arrow) and at their normal site. Additionally, innervation from the spiral ganglion
897 was observed in the hair cell part and in Kölliker's organ in the middle and apical of the cochlea
898 (arrowheads and brackets). **B**. Low-magnification view of the basal region of the whole mount
899 cochlear image in E18.5 *Ebf1*$^{+/+}$ and *Ebf1*$^{-/-}$ mice labeled with TUJ1 (green). **C**. High-
900 magnification view of the basal region of the whole mount cochlear image in E18.5 *Ebf1*$^{+/+}$ and
901 *Ebf1*$^{-/-}$ mice labeled with TUJ1 (green) and MYO7A (gray). In *Ebf1*$^{+/+}$ mice, the neurons ran
902 parallel to the outer hair cells, whereas in *Ebf1*$^{-/-}$ mice, the neurons formed a reticulation within
903 the cochlear hair cell regions. Scale bars: 100 μm in **A** and 20 μm in **B** and **C**.

Figure 9. *Ebf1* deletion causes JAG1 expression to spread inward, delaying *Atoh1* expression during cochlear development.

A. Results of *in situ* hybridization of *Fgf10* and *Bmp4* and immunostaining of JAG1 (green) on cross sections of the basal-to-middle region of the cochlea of $Ebf1^{+/+}$ and $Ebf1^{-/-}$ mice at embryonic day (E) 13.5 and E14.5. The prosensory domain is shown in brackets. **B**. Result of *in situ* hybridization of *Atoh1* on cross sections of the basal-to-middle region of the cochlea of $Ebf1^{+/+}$ and $Ebf1^{-/-}$ mice at E14.5 and E15.5. Areas enclosed by dashed lines indicate cochlear ducts and vestibules. Scale bars: 100 μm.

Figure 10. Effect of *Ebf1* deletion on cell proliferation during inner ear development.

A. Cross sections of the cochlear basal regions at embryonic day (E) 12.5, E13.5, E14.5, and E16.5 from $Ebf1^{+/+}$ and $Ebf1^{-/-}$ mice. Sections were immunostained with 5-ethynyl-2'-deoxyuridine (EdU, green) and SOX2 (magenta). E16.5 sections were counter-stained with 4',6-diamidino-2-phenylindole (DAPI, gray). Areas enclosed by dashed lines indicate the cochlear ducts and brackets indicate prosensory domains. **B**–**D**. Quantitative assessment of the SOX2-positive region in the cochlea epithelia. The numbers of SOX2-positive cells (**B**) as well as EdU- and SOX2-double positive cells (**C**) were counted, and the percentage of EdU-positive cells among SOX2-positive cells (**D**) was calculated. Error bars represent mean ± standard deviation (n = 4). **E**. Cross sections of the cochlear basal regions at E13.5 and E14.5 from $Ebf1^{+/+}$ and $Ebf1^{-/-}$ mice immunostained with CDKN1B (green) and SOX2 (magenta). **F**. Quantitative assessment of the CDKN1B-positive region in the cochlear epithelia. The numbers of CDKN1B- and SOX2-doule positive cells were counted. Two-way ANOVA with Bonferroni *post-hoc* test

(**B**, **C** and **D**) and Student's *t*-test (**F**) were performed. $^{**}p < 0.01$, $^{***}p < 0.001$, and $^{****}p < 0.0001$. Error bars represent mean ± standard deviation (n = 4 for **B**, **C**, **D**, and **F** (E14.5), n = 3 for **F** (E13.5)). Scale bars: 100 μm.

Figure 11. *Ebf1* deletion did not affect apoptosis during inner ear development.

Cross sections of the embryonic day (E) 11.5 inner ear and E13.5 cochlear basal region from *Ebf1*$^{+/+}$ and *Ebf1*$^{-/-}$ mice. Sections were labeled with cleaved caspase 3 (CC3, green) and 4',6-diamidino-2-phenylindole (DAPI, blue). The number of CC3-positive cells was similar between *Ebf1*$^{-/-}$ and *Ebf1*$^{+/+}$ mice at E11.5 and E13.5. Scale bars: 100 μm.

Figure 12. *Ebf1* deletion impairs auditory function.

A. Auditory brainstem response (ABR) thresholds of P21 *Foxg1Cre;Ebf1*$^{fl/fl}$ (Cre;EBF1$^{fl/fl}$) (dashed line) and *Foxg1Cre;Ebf1*$^{fl/+}$ (Cre;EBF1$^{fl/+}$, control) (solid line) mice. **B**. Distortion product optoacoustic emissions (DPOAE) were measured at P21 from *Foxg1Cre;Ebf1*$^{fl/fl}$ (dashed line) and control (solid line) mice. $^{*}p < 0.05$, $^{**}p < 0.01$, and $^{****}p < 0.0001$ from one-way ANOVA with Tukey-Kramer *post-hoc* test. Error bars represent mean ± standard error of mean (n = 3 for **A** and n = 4 for **B**). **C**. The whole mount images of the cochlear basal regions from *Foxg1Cre;Ebf1*$^{fl/+}$ and *Foxg1Cre;Ebf1*$^{fl/fl}$ mice at P23 labeled with phalloidin (green). Scale bar: 20 μm.

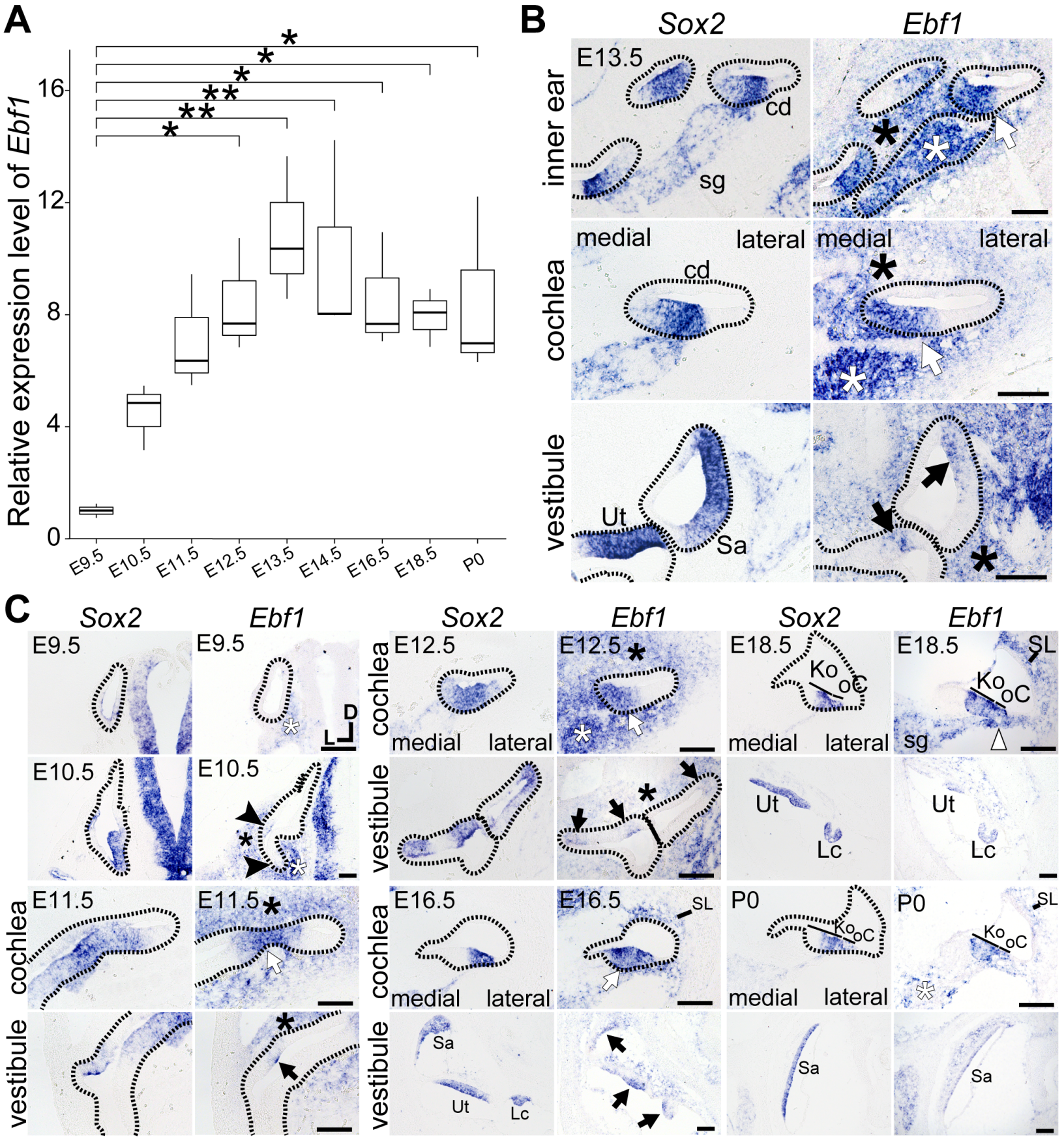
A
Relative expression level of Ebf1
0
4
8
12
16
E9.5
E10.5
E11.5
E12.5
E13.5
E14.5
E16.5
E18.5
P0
B
Sox2
Ebf1
inner ear
cochlea
vestibule
E13.5
cd
sg
medial
lateral
Ut
Sa
C
Sox2
Ebf1
E9.5
E10.5
E11.5
E12.5
E16.5
E18.5
P0
cochlea
vestibule
medial
lateral
D
L
Ko
oC
SL
sg
Ut
Lc
Sa

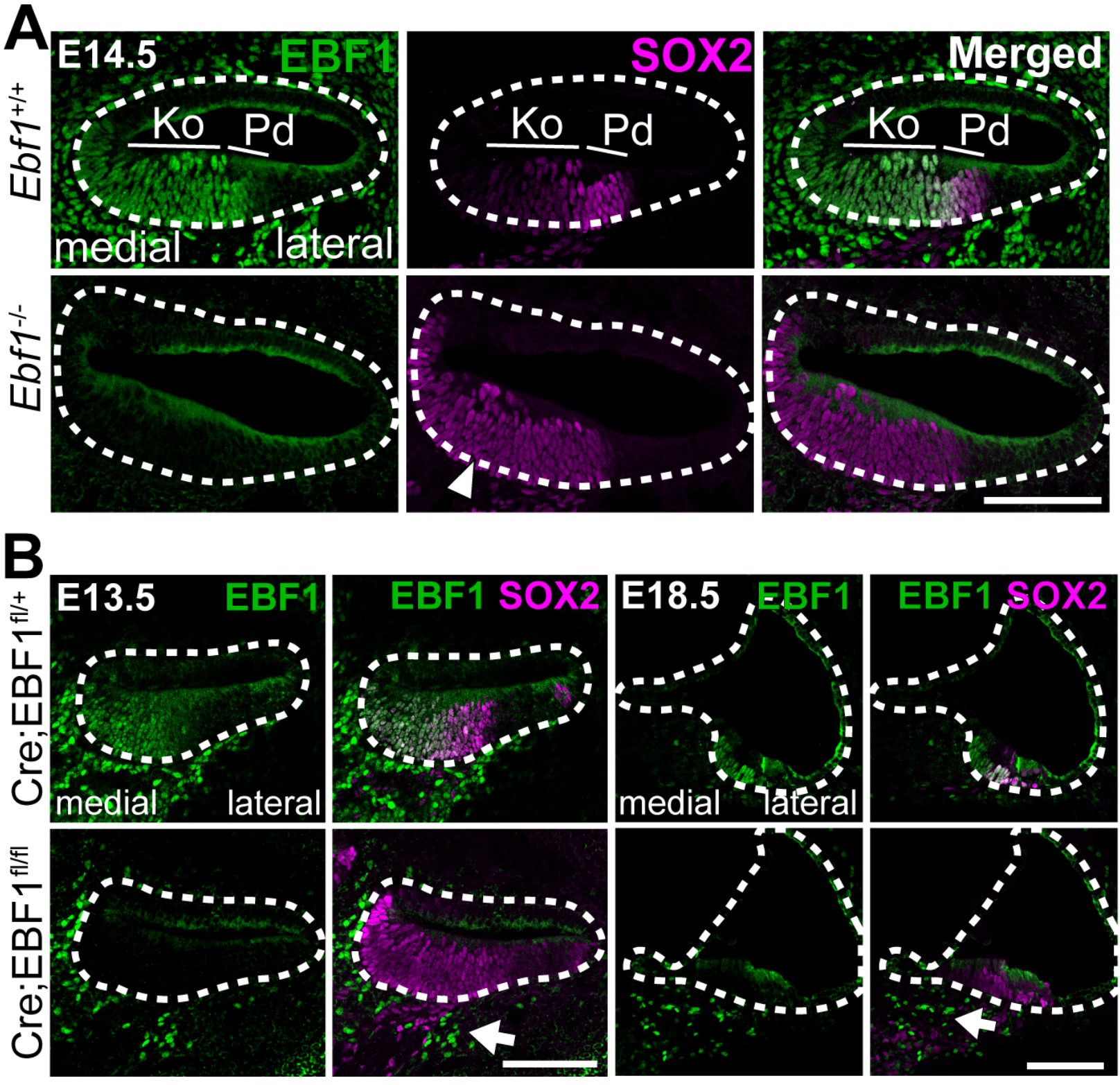
A
E14.5
EBF1
SOX2
Merged
Ko
Pd
medial
lateral
Ebf1+/+
Ebf1-/-
B
E13.5
EBF1
EBF1 SOX2
E18.5
Cre;EBF1fl/+
Cre;EBF1fl/fl

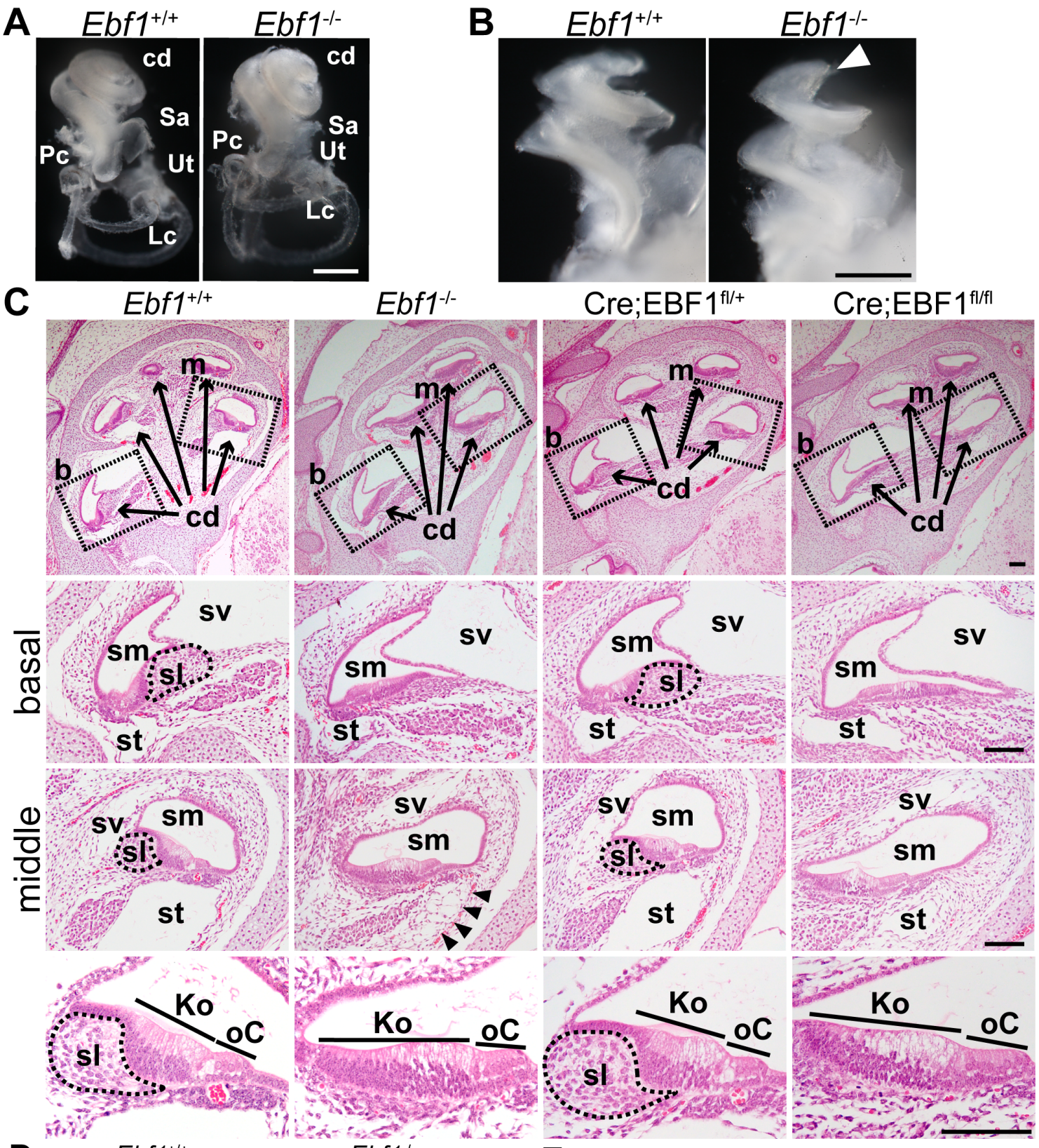
A
Ebf1+/+
Ebf1-/-
cd
Sa
Pc
Ut
Lc
B
Ebf1+/+
Ebf1-/-
C
Ebf1+/+
Ebf1-/-
Cre;EBF1fl/+
Cre;EBF1fl/fl
m
b
cd
basal
middle
sv
sm
sl
st
Ko
oC
D
Ebf1+/+
Ebf1-/-
E18.5 FABP7 MYO7A
Ko
oC
Cre;EBF1fl/+
Cre;EBF1fl/fl
E
Ebf1+/+
Ebf1-/-
Cre;EBF1fl/+
Cre;EBF1fl/fl
area of spiral limbus
μm2
10000
5000
0
*
**
**
**
basal
middle
basal
middle

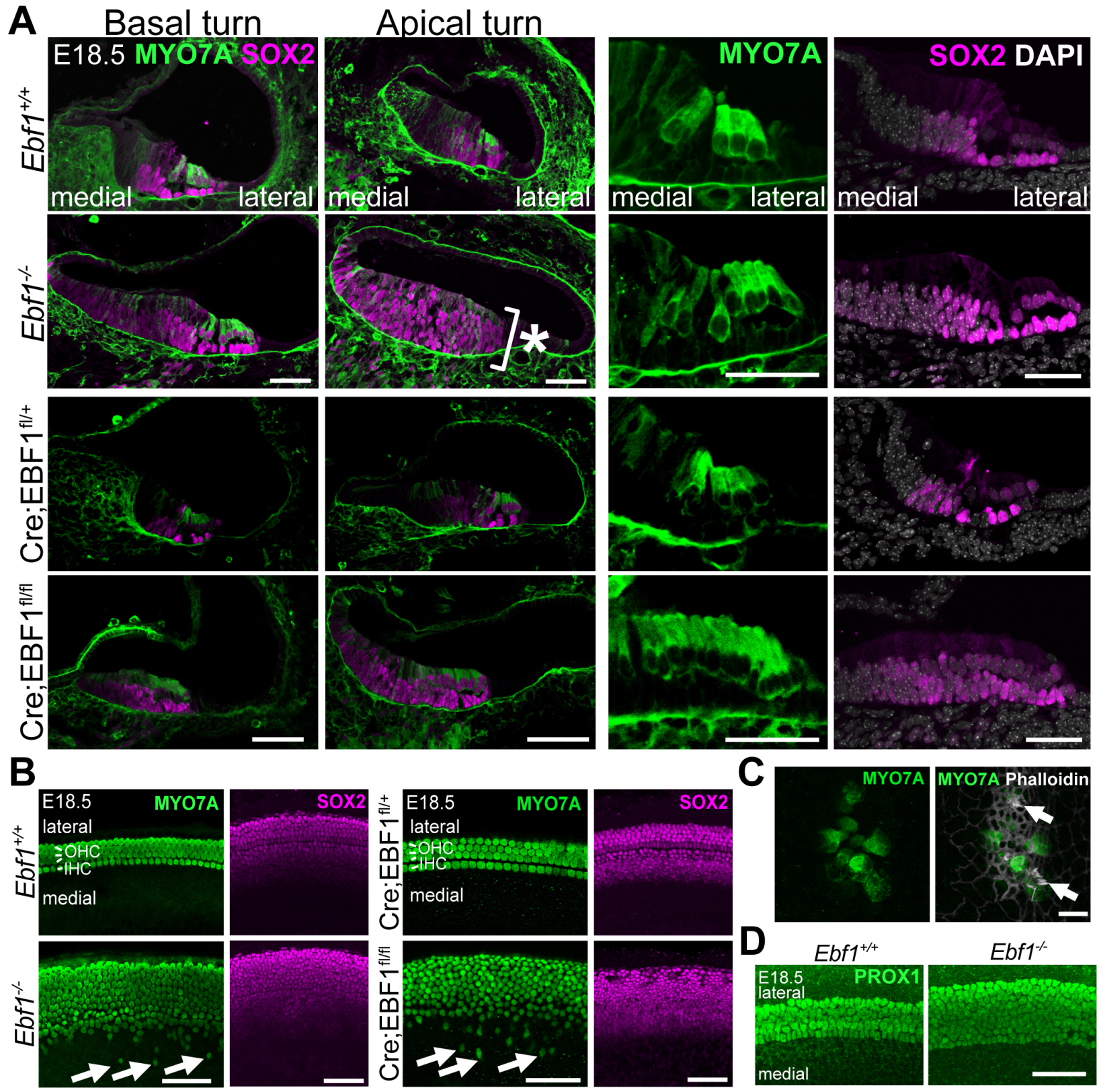
A
Basal turn
Apical turn
E18.5 MYO7A SOX2
MYO7A
SOX2 DAPI
medial
lateral
Ebf1+/+
Ebf1-/-
Cre;EBF1fl/+
Cre;EBF1fl/fl
*
B
E18.5
MYO7A
SOX2
lateral
OHC
IHC
medial
C
MYO7A
MYO7A Phalloidin
D
Ebf1+/+
Ebf1-/-
E18.5
PROX1
lateral
medial

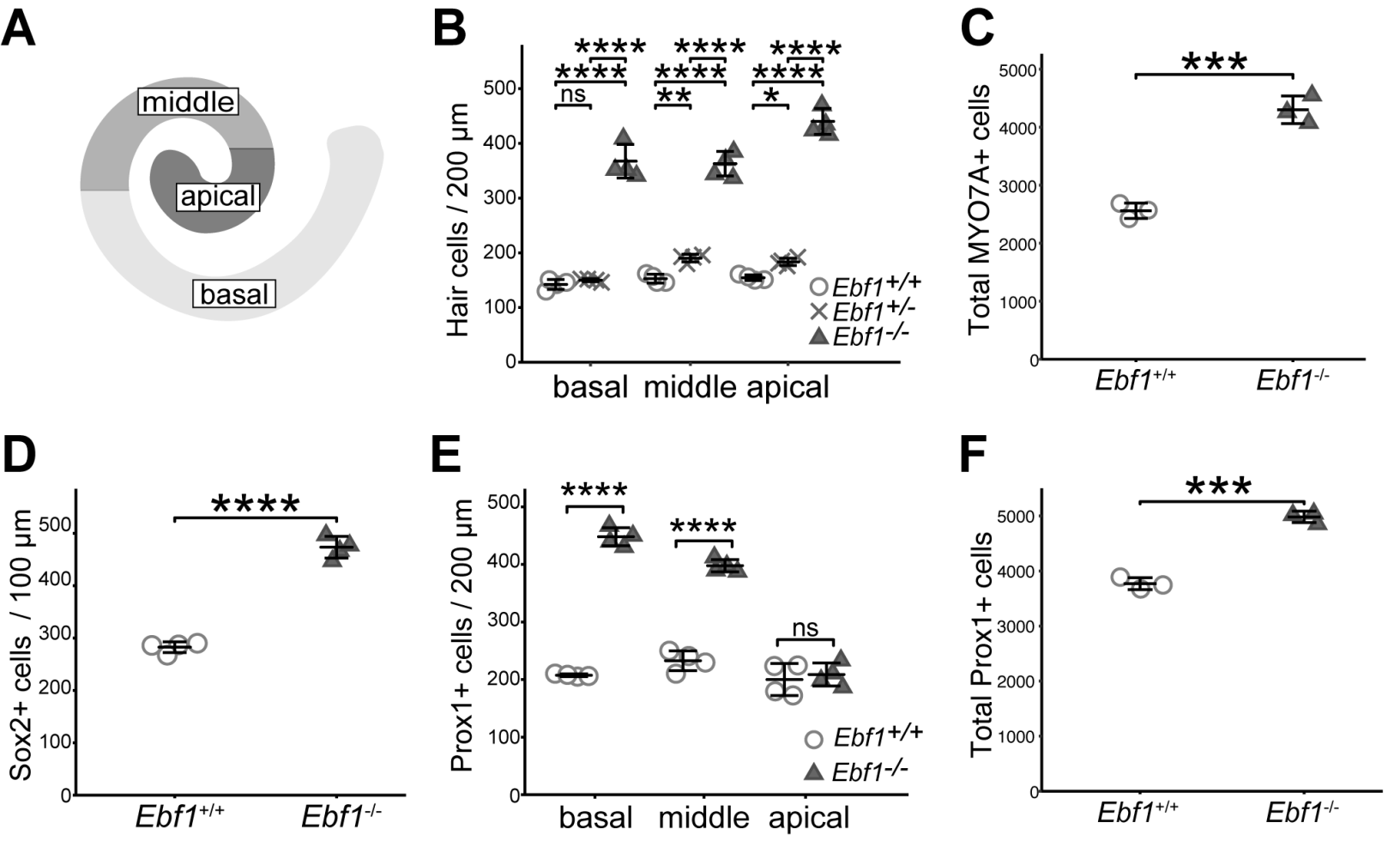
A
middle
apical
basal
B
Hair cells / 200 µm
****
****
****
****
****
****
ns
**
*
Ebf1+/+
Ebf1+/-
Ebf1-/-
basal middle apical
C
Total MYO7A+ cells
***
Ebf1+/+
Ebf1-/-
D
Sox2+ cells / 100 µm
****
Ebf1+/+
Ebf1-/-
E
Prox1+ cells / 200 µm
****
****
ns
Ebf1+/+
Ebf1-/-
basal middle apical
F
Total Prox1+ cells
***
Ebf1+/+
Ebf1-/-

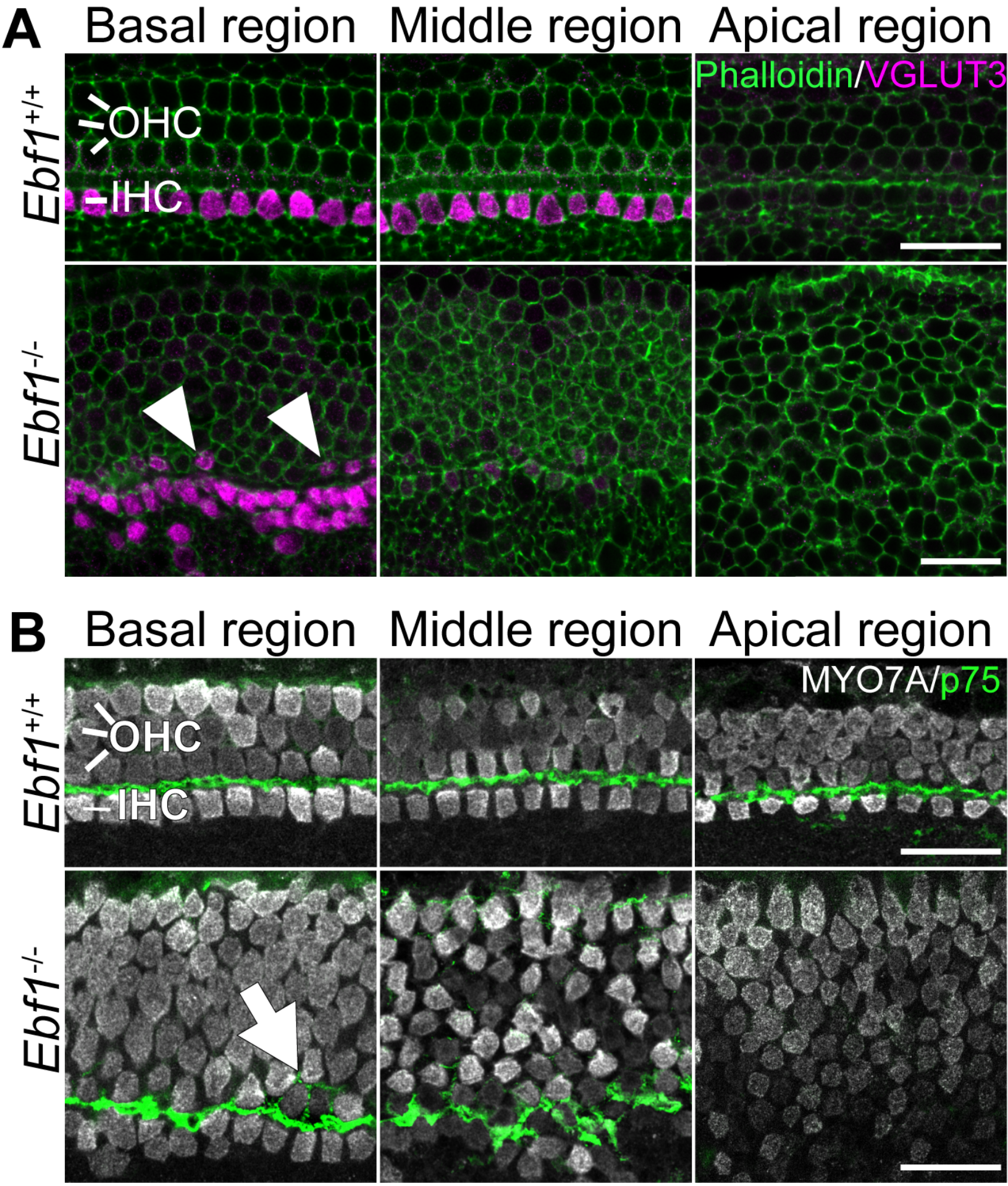
A
Basal region
Middle region
Apical region
Phalloidin/VGLUT3
Ebf1+/+
OHC
IHC
Ebf1-/-
B
Basal region
Middle region
Apical region
MYO7A/p75
Ebf1+/+
OHC
IHC
Ebf1-/-

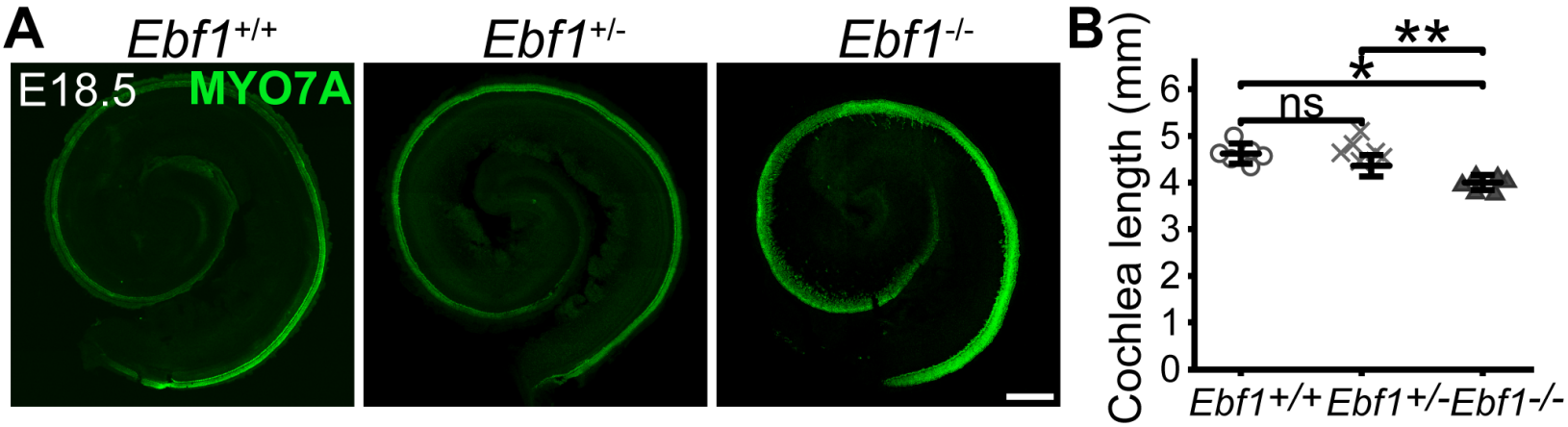
A
Ebf1+/+
Ebf1+/-
Ebf1-/-
E18.5
MYO7A
B
Cochlea length (mm)
0
1
2
3
4
5
6
ns
*
**
Ebf1+/+
Ebf1+/-
Ebf1-/-

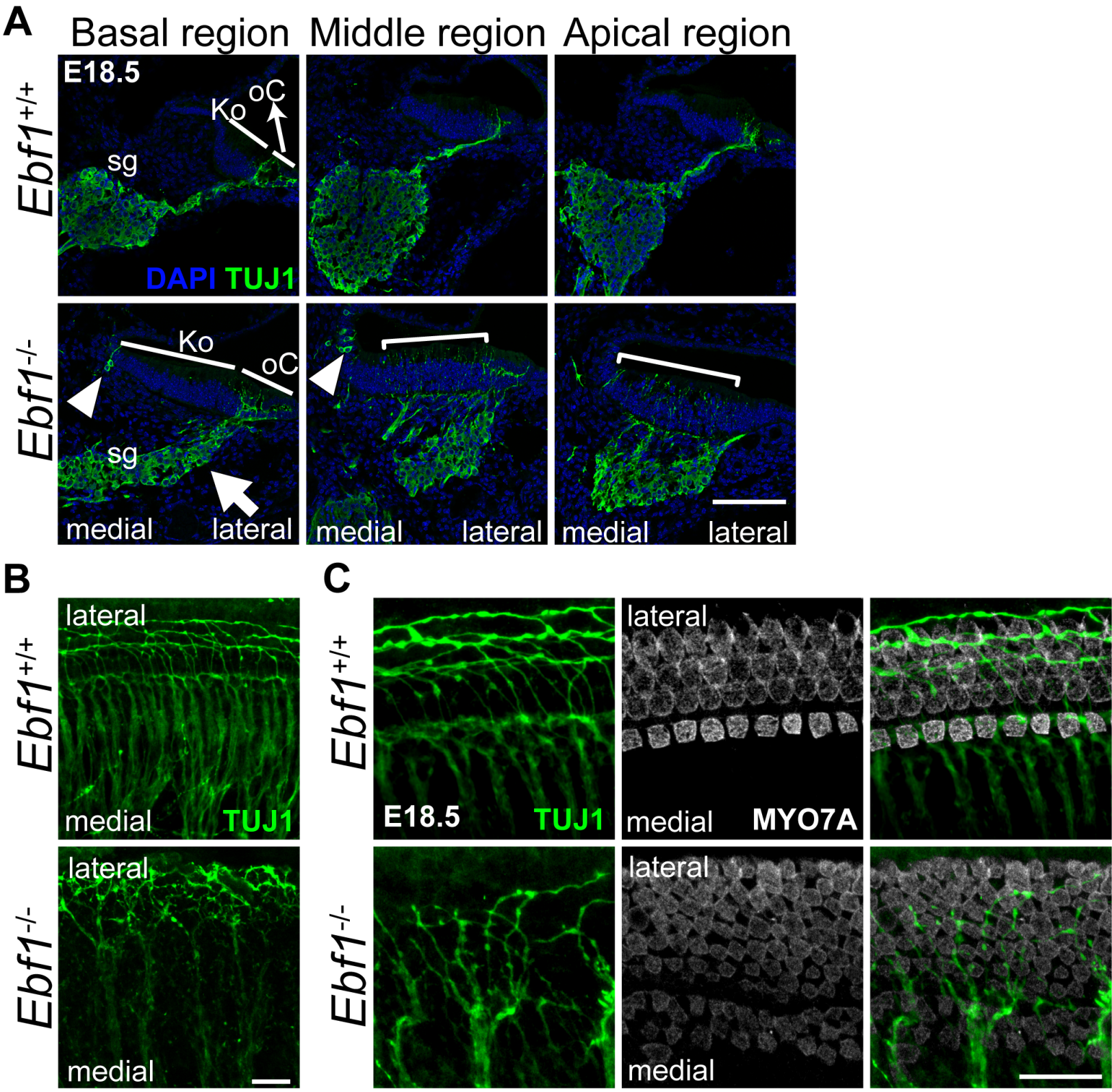
A
Basal region
Middle region
Apical region
E18.5
Ebf1+/+
Ebf1-/-
Ko
oC
sg
DAPI TUJ1
medial
lateral
B
C
TUJ1
MYO7A

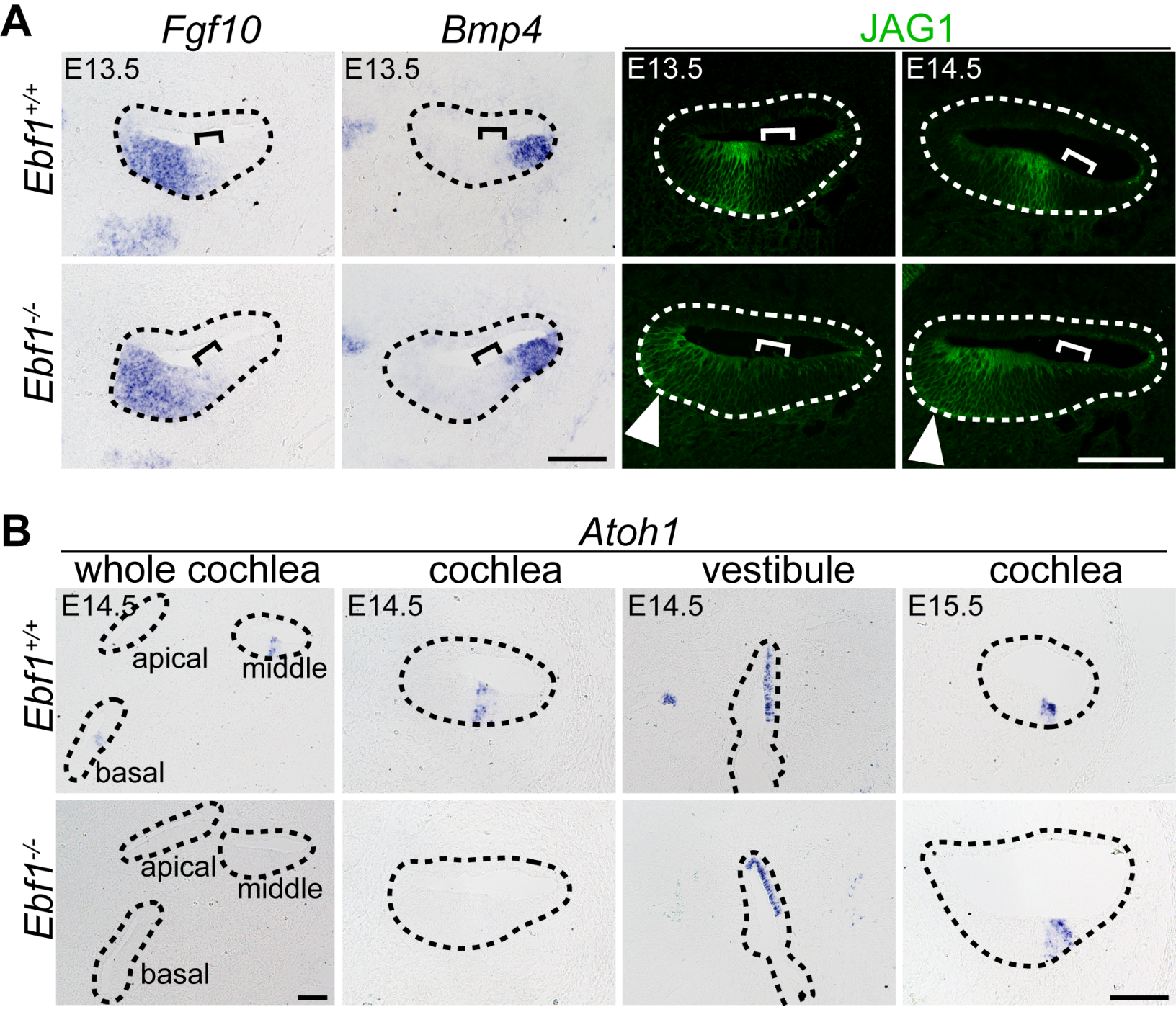
A
Fgf10
Bmp4
JAG1
E13.5
E13.5
E13.5
E14.5
Ebf1+/+
Ebf1-/-
B
Atoh1
whole cochlea
cochlea
vestibule
cochlea
E14.5
E14.5
E14.5
E15.5
apical
middle
basal
apical
middle
basal

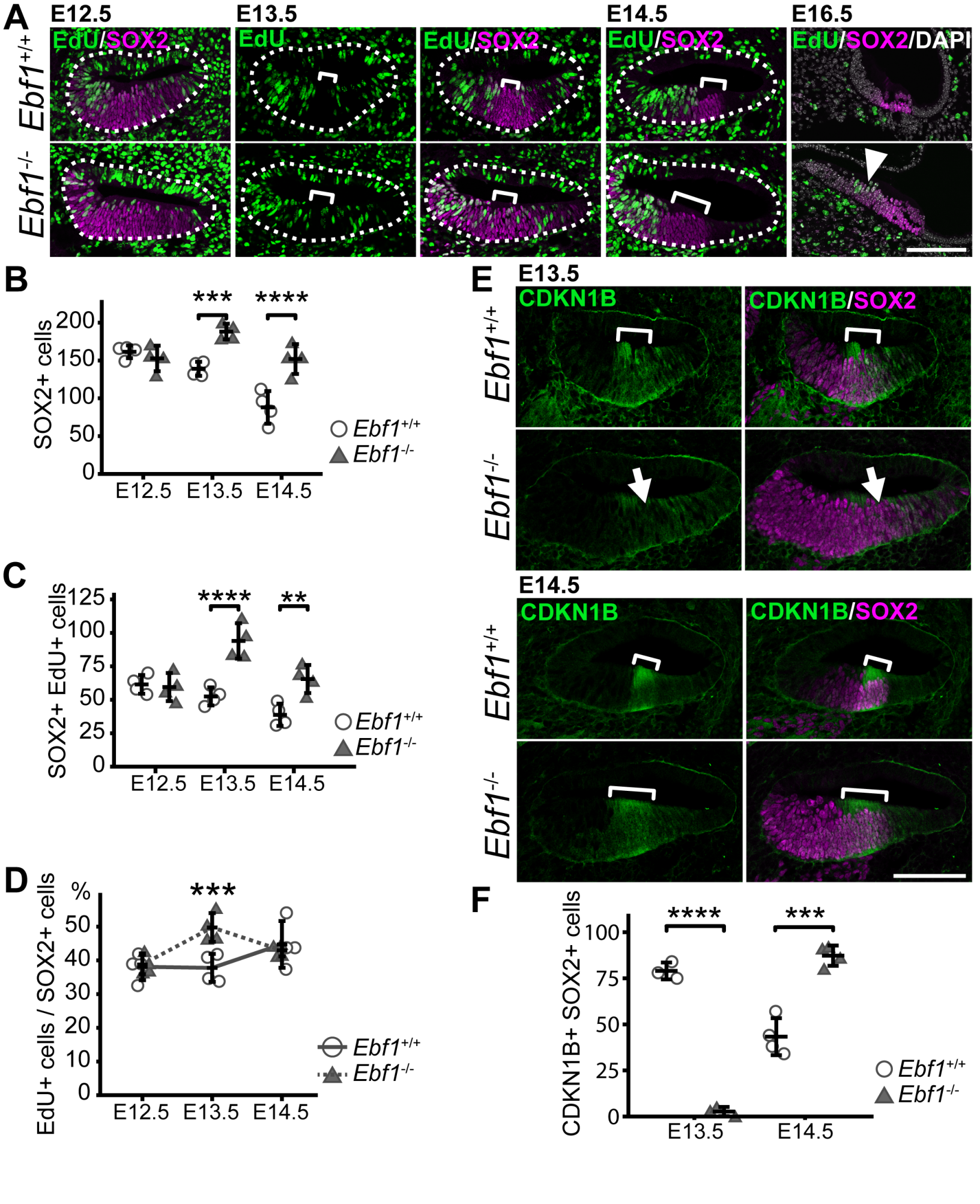
A
E12.5
E13.5
E14.5
E16.5
EdU/SOX2
EdU
EdU/SOX2
EdU/SOX2
EdU/SOX2/DAPI
Ebf1+/+
Ebf1-/-
B
SOX2+ cells
200
150
100
50
0
***
****
E12.5
E13.5
E14.5
Ebf1+/+
Ebf1-/-
C
SOX2+ EdU+ cells
125
100
75
50
25
0
****
**
E12.5
E13.5
E14.5
Ebf1+/+
Ebf1-/-
D
EdU+ cells / SOX2+ cells
%
50
40
30
20
10
0
***
E12.5
E13.5
E14.5
Ebf1+/+
Ebf1-/-
E
E13.5
CDKN1B
CDKN1B/SOX2
Ebf1+/+
Ebf1-/-
E14.5
CDKN1B
CDKN1B/SOX2
Ebf1+/+
Ebf1-/-
F
CDKN1B+ SOX2+ cells
100
75
50
25
0
****
***
E13.5
E14.5
Ebf1+/+
Ebf1-/-

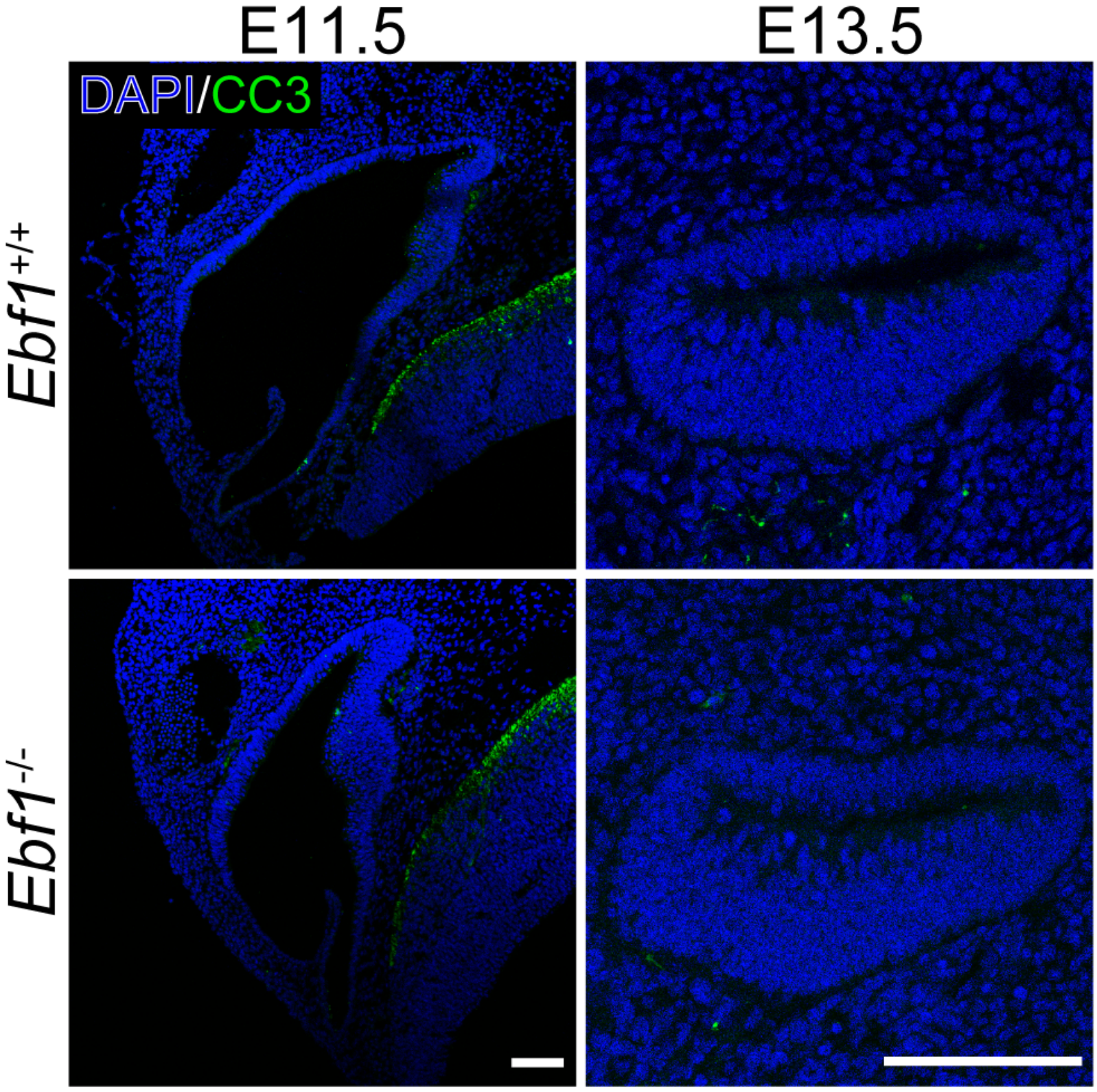
E11.5
E13.5
DAPI/CC3
Ebf1+/+
Ebf1-/-

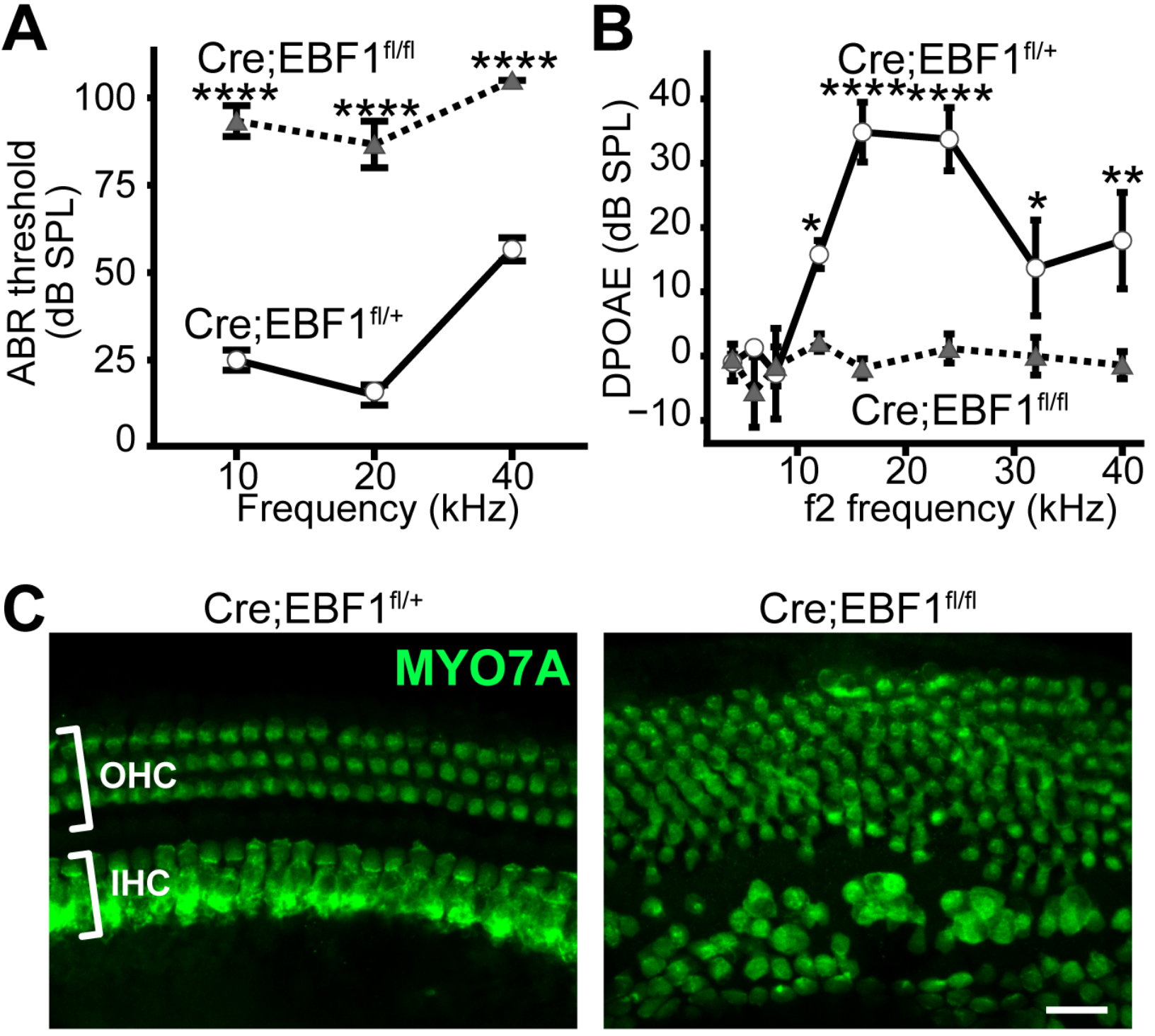
A
Cre;EBF1fl/fl
Cre;EBF1fl/+
ABR threshold (dB SPL)
100
75
50
25
0
10
20
40
Frequency (kHz)
****
****
****
B
Cre;EBF1fl/+
Cre;EBF1fl/fl
DPOAE (dB SPL)
40
30
20
10
0
−10
10
20
30
40
f2 frequency (kHz)
*
****
*
**
C
Cre;EBF1fl/+
Cre;EBF1fl/fl
MYO7A
OHC
IHC